VYSOKÉ UČENÍ TECHNICKÉ V BRNĚ
Fakulta chemická
Ústav fyzikální a spotřební chemie

Ing. Ota Salyk, CSc.

THIN FILMS DEPOSITION OF AMORPHOUS SILICON AND ORGANOSILICON COMPOUNDS

PŘÍPRAVA TENKÝCH VRSTEV AMORFNÍHO KŘEMÍKU A ORGANOKŘEMIČITÝCH SLOUČENIN

SHORT VERSION OF HABILITATION THESIS
VĚDNÍ OBOR : MATERIÁLOVÉ INŽENÝRSTVÍ

VUTIUM

BRNO 2003

KEY WORDS

Adhesion, amorphous hydrogenated silicon, chemical vapor deposition, composite material, desorption, electroluminescence, electron beam evaporation, evaporation, hydrogen, indium-tin oxide, infrared absorption spectroscopy, ion source, light emitting diode, luminescence, mass spectroscopy, microwave plasma, optical absorption spectroscopy, plasma, polysilane, polysiloxane, rf plasma, silicon, thin film, vacuum

Adheze, amorfní hydrogenovaný křemík, depozice z plynné fáze, desorpce, electroluminiscence, hmotnostní spektrometrie, indium-cín oxid, infračervená absorpční spektroskopie, iontový zdroj, kompozitní materiál, křemík, luminiscence, mikrovlnné plazma, napařování elektronovým svazkem, napařování, vodík, optická absorpční spektroskopie, plazma, polysilan, polysiloxan, radiofrekvenční plazma, svítivka, tenká vrstva, vakuum.

Habilitation thesis is placed in the Institute of Physical and Applied Chemistry at Faculty of Chemistry of Brno University of Technology, Purkyňova 118, Brno.

Práce je uložena na Ústavu fyzikální a spotřební chemie Fakulty chemické Vysokého učení technického v Brně, Purkyňova 118, Brno.

Acknowledgments

I would like to express my acknowledgements to Prof. František Schauer, DrSc. for good management of the research, to which the first three topics of this work were devoted and As. Prof. Vladimír Čech for the leadership of the research program through which the topic of the forth part originated. I would also like to thank my colleagues who supported the research described in this thesis in various ways, in particular Dr. Aleš Poruba, Dr. Pavel Horváth, Dr. Martin Weiter, Mgr. Ivo Kuřitka and Mgr. Radek Přikryl. My thanks go also to the Faculty of Chemistry staff, Brno University of Technology for their collaboration and providing a pleasant atmosphere at the institute.

Last but not least, I want to thank all members of my family, especially my wife Zdeňka Říhová, for their patience, tolerance and support.

ISBN 80-214-2283-1
ISSN 1213-418X

CONTENT

Author's introduction

Dr. Ota Salyk was born 1954 in Český Těšín. (Czech Republic), where he lived and acquired primary and secondary education at the secondary grammar school. Now he lives in Brno. He is married and has four children.

In 1978 he graduated at the Faculty of Electrical Engineering, the orientation of his study was electro-technology and microelectronics with the diploma project "Fluctuation Phenomena in Magnetic Materials".

Since 1978 he was engaged at the Institute of Scientific Instruments of the Czechoslovak Academy of Sciences in Brno, firstly focusing on detectors of electrons for scanning electron microscopy, later on electron emission from lanthanum hexaboride cathodes and from tunneling structures Al-Al_2O_3-Au.

In 1983 he joined the Department of Physics of the Technical Academy, as lecturer of physics.

In 1988 he defended his PhD thesis on "Preparation and Properties of Evaporated Amorphous Silicon" His main activities include the deposition techniques of thin films and some characterization techniques. He has specialized on the development of vacuum and plasma equipment like electron gun for evaporation, microwave electron cyclotron resonance discharge apparatus, ion source etc.

In 1993 he proceeded to the Brno University of Technology, Faculty of Chemistry, Institute of Physical and Applied Chemistry where he has been working until now as the physics lecturer. Here he has been engaged in several professional branches: vacuum evaporation, plasma chemical vapor deposition of polysilanes, polysiloxanes and plasma treatment of various materials. He continued in vacuum and low temperature plasma topics for several research purposes. In this new employment he constructed the high-pressure rf plasmatron for plasma treatment of powder substances in chemistry, apparatus for thermal desorption spectroscopy, he took part on construction of other vacuum equipment for rf discharges and the thin films adhesion tester - the scratch tester.

Apart from that he delivers the course of physics and plasma physics for undergraduate students and also some topics of vacuum deposition techniques for PhD. students. He is a chief lecturer in the laboratory of physics, which was established and developed under his management. He contributed to it by several original physics experiments and a book of laboratory experiments for students.

Dr. Salyk is the author and co-author of more than 40 papers in journals and conferences, 2 patents and 15 research reports. He took part on 13 grants and as a main coordinator at 4 of them he delivered and defended the final report.

INTRODUCTION

Presented work is devoted to four continuing themes of thin films preparation and vacuum and plasma technology acquired in plasma laboratory of the faculty workplace. All these topics concern silicon based compounds and are joined by common methods of preparation and examination. The emphasis is directed on preparation techniques, where the vacuum and plasma technologies prevail. Several original equipments for thin films deposition and testing were developed for this reason and are described in the thesis.

The first part is devoted to amorphous silicon deposition, its deposition equipment and processes of thin film growth and its hydrogenation. Hand by hand with the material their preparation techniques were developed. The classical physical vapor deposition was not convenient for a-Si:H preparation, so the chemical vapor deposition techniques spread widely. The a-Si:H thin film of device quality was first prepared by decomposition of silane in 1965 by Stearling and Swann [1] through a radiofrequency glow discharge in SiH_4. In 1975 Spear and LeComber [2] were the first who systematically reported doping of a-Si:H by p-type and n-type over a large range by addition of doping gases phosphine and diborane into the discharge. Once this was possible, the material became suitable for various applications and soon the first products such as e.g. solar cells based on a-Si:H were reported by RCA laboratories. The disadvantage of characterization and it contains the main results of the research work in the last ten years in this material fabrication was the low deposition rate ($0.3\ nm\ s^{-1}$) so alternative techniques were developed. One of them is decomposition of silane in microwave discharges (Mishima and Kiuchi in 1983 [3]) and application of the electron cyclotron resonance microwave discharge (Matsuo et al. in 1983 [4]). The subsequent following deposition hydrogenation was carried out by ion beam implantation from the Kaufmann's type ion sources [5]. In multilayer device fabrication some other techniques should be used like substrate cleaning, treatment, contacts deposition, device pasivating and protecting, which were developed as well.

The second part is devoted to the thermal desorption spectroscopy, a method and equipment for analysis of desorbed gases from thin films when they are heated. The method was developed for evolution examination of amorphous hydrogenated silicon and later it was applied to some plasma polymer thin films.

The third part concerns preparation technique and fundamental properties of polysilane thin films deposited by vacuum evaporation and plasma polymerization. Independently of silicon based materials and other inorganic semiconductors the various semiconducting organic materials enticed since seventies of the last century. The use of organic semiconductors in light-emitting diodes (LEDs) has probably generated the most interest till now. The earliest report of electroluminescence (EL) from an organic material was made in 1963 by Pope et al., who observed EL from 10-20 mm thick crystals of anthracene at voltages above 400 V [6]. Two decades later, the results of Tang and Van Slyke [7] and Adachi et all. on EL from thin sublimed multilayer organic films were a substantial advance towards a practical organic EL technology [8]. This work showed that organic amorphous active materials could be used to realize stable devices with high quantum efficiencies. These results spurred worldwide interest in organic materials for light−emitting diode research [9]. Most of these materials are soluble and enable preparation of coatings from solution by casting and spin coating technique. In some cases Langmuir-Blodgets films were prepared and also vacuum evaporation was used.

Besides low molecular weight materials attention was also focused on polymers because of the possibility to transport carriers along the polymer chain. There are numerous organic materials, which can be regarded as electroactive polymers, i.e., polymers that exhibit some electronic properties. In the field of electroluminescent materials two meaningful groups can be mentioned: a polymers with π-conjugated backbones and polymers with σ-conjugated backbones. In contrast to conventional conjugated polymers, polysilylene polymers exhibit the σ-electron delocalization

along the polymer chain with catenated Si-Si bonds. In this thesis the polysilylenes are of considerable research interest, especially the poly(methylphenylsilylene) (PMPSi) and poly(dimethylsilylene) (PDMSi). The σ-conjugated polysilanes are anomalous due to light emission in ultraviolet region.

Polysilanes are quasi-one-dimensional Si-backbone polymers with alkyl or aryl groups as side chains. Their physical properties are strongly influenced by the chemical structure of the polymer side group. They are prepared from solution by the spin coating methods, but also in case of bad solubility by vacuum evaporation [10]. The evaporation of the polymer is accompanied by its decomposition and the resulting condensed films have an oligosilanes character with similar electronic properties to the original polymer. So also oligosilanes prepared synthetically are studied [11].

The forth part is devoted to instrumentation of siloxanes plasma polymerization. The plasma polymerization provides also thin films of excellent mechanical properties, like adhesion, flexibility and environmental resistance. Its behavior is influenced by plasma substrate surface activation and subsequent chemical bonding of plasma polymer. Also the outer surface remains activated for further layer deposition. This property can be used for fiber reinforced composites, where the plasma polymer can play a role of interphase between the reinforcement and the matrix [12], [13] and [14].

Through these topics, the plasma reactor enabling plasma polymer deposition onto glass flat substrates and infinity glass fibers was developed. The plasma environment was examined by mass spectroscopy and the appropriate conditions were adjusted. The resulting thin films were tested for adhesion on own scratch-tester developed for this purpose.

1 PREPARATION OF AMORPHOUS SILICON

Amorphous silicon is over-coordinated substance as its average bond number is close to 4 like in a single silicon atom and the consequence of this is large internal stress leading to dangling bond creating. Their concentration in amorphous silicon a-Si usually does not exceed $10^{20}cm^{-3}$. Energy of electrons of these dangling bonds is dispersed in the region of forbidden gap of crystalline silicon and their concentration is big enough to cause hopping conductivity. Moreover, Si atom with dangling bond can be in three charge states – neutral, positively and negatively charged. If these dangling bonds are saturated by hydrogen, energy of bonding electrons falls deep into valence band.

Electronic grade material demands low density of states (DOS) of order $10^{16}cm^{-3}eV^{-1}$ which can be achieved by technique of low energy physical or chemical vapor deposition. Resulting thin film should have low internal stress to avoid dangling bonds creation. In a-Si:H motion of hydrogen plays a role in defect creation under, for example, illumination (Staebler–Wronski effect), carrier injection and temperature cycling [15]. It is important to optimize hydrogen incorporation into the layer.

According to Jackson and Zhang [16] H is predominantly bonded in the silicon monohydride form SiH and the remainder in SiH_2 and SiH_3 groups that can be localized in pairs on sites of broken weak Si—Si bonds.

1.1 OVERVIEW OF PREPARATION TECHNIQUES OF AMORPHOUS HYDROGENATED SILICON

Amorphous hydrogenated silicon (a-Si:H) can be prepared on large area substrates. It determinates its application for solar cells and display electronics including flat screens for switching luminescent elements. Since 1975 [2] economically profiting techniques for large area preparation of solar cells were being developed resuming high quality material with low DOS. Contemporary method PE CVD (Plasma Enhanced Chemical Vapor Deposition) called also GD

(Glow Discharge) from silane (SiH_4) provided high quality low DOS material, but at low power discharge giving deposition rates below 0.3 nm s^{-1}. Increasing power and pressure leads to volume decomposition of silane. Quick overview of most widespread methods is in following scheme in Fig. 1.1.

Contemporary methods used in the solar cells production prefer CVD methods. High deposition rate methods were developed by using microwave discharges or RF CVD on higher frequencies. For solar cells production at least three-layer structure (PIN diode) is necessary besides passivating, protecting and contacting layers. They are produced in multi-chamber reactor systems on stainless steel plates, glass tiles, kapton foils etc. The most important technical parameter is their efficiency. Contemporary steady state value is about 10 %. It is still increasing by suppressing so-called Staebler-Wronski effect [15] that causes material degradation, and by improving lateral homogeneity on large areas.

In our laboratory there were developed some alternative methods of amorphous silicon deposition. Mainly it was electron beam evaporation with hydrogenation from MW ECR (micro–wave electron cyclotron resonance) plasma source or MW ECR ion gun, MW ECR PA CVD (plasma assisted chemical vapor deposition) from silane decomposition and RF PA CVD (radio–frequency) from silane at capacitively coupled 13,56 MHz discharge. The description of some components developed and tested in our laboratory follows below.

1.2 MICROWAVE MAGNETOACTIVE PLASMA SOURCE

1.2.1 Physical background

The overview of temporary state of art of micro–wave plasma sources is in [17]. For microwave plasma sources it is important a kind of microwave excitation [18]. The most frequently we can encounter open system, where the wave–guide is followed by a discharge chamber or a ray antenna. Recombination in plasma can be limited by an appropriate magnetic field. The convenient means fulfilling this demand is space orientation of magnetic field strength $\boldsymbol{B_0}$ perpendicular to electric field strength $\boldsymbol{E}$ of micro–wave. So-called magnetoactive plasma is created, where the diffusion conditions are variable. In such case the plasma density can reach values of up to 100 critical values in isotropic plasmas.

In case of magnetic field strength $B_0 = B_{ce}$,

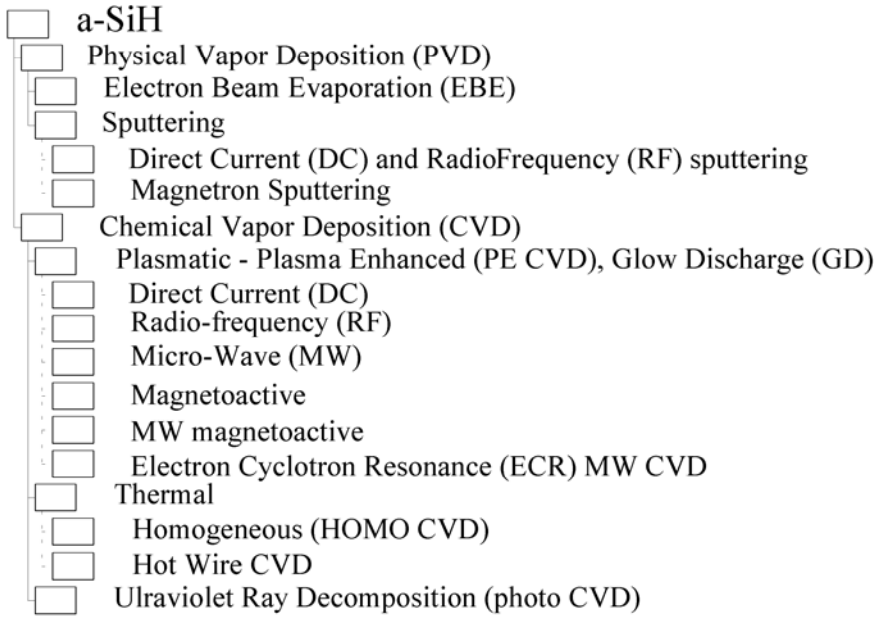

Fig. 1.1 Quick overview of most widespread methods is in depicted scheme

$$B_{ce} = \frac{2\pi f m_e}{e}, \tag{1.1}$$

so called electron cyclotron resonance (ECR) occurs (B_{ce} = 0.0875 T for frequency 2.45 GHz). Absorption in regime of ECR enables to generate plasma in wide range of pressures 10^{1} to 10^{-3} Pa. Plasma density at micro–wave power of range of 1 kW can achieve $n = 10^{12}$cm^{-3}.

From the ECR region plasma is accelerated against the direction of magnetic field gradient because of its diamagnetic character. Accelerating force works on electron

$$\mathbf{F} = -\mu \operatorname{grad} \mathbf{B}_0, \tag{1.2}$$

where

$$\mu = \frac{m_e v_\perp^{\ 2}}{2B_0}. \tag{1.3}$$

μ is magnetic momentum of electron and $v_\perp$ is component of electron velocity perpendicular to lines of induction. Because ions are forced to follow electrons out of ECR region by space charge of electrons, velocities of both electrons and ions are the same. The open system with axial magnetic field was chosen in our case. Its description follows.

1.2.2 Project of plasma source

The design of microwave ECR plasma source is apparent from Fig. 1.2 and Fig. 1.10. It consists of several parts designed separatively. The discharge chamber is a quartz glass bell jar of diameter 80 mm with cone termination connected to the processing chamber by Viton "O" ring sealing, pushing ring and a ring flange. It is inside a cylindrical wave–guide adapted by its

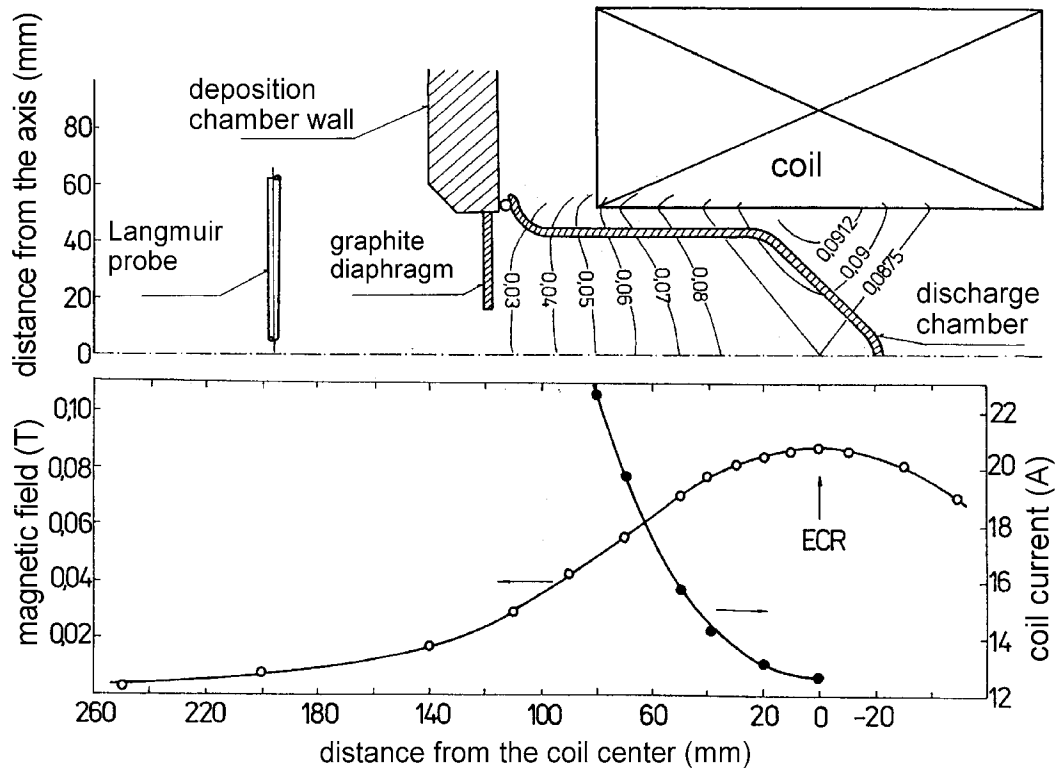

Fig. 1.2 Axis cross-section of microwave magnetoactive plasma source ant the magnetic field strength distribution along the axis. ○– magnetic field strength on the axis at coil current 12.6 A (B_{ce}=0.0875 T). ●–position of ECR on the axis of the discharge chamber vs coil current

diameter of 100 mm to frequency 2.45 GHz. Its length is 500 mm and it is ended by the tuning piston. There is magnetron Hitachi 2M107A with maximum power 700 W introduced through antenna into the wave-guide.

Magnetron is supplied from the current power supply with the near constant maximum voltage 3.3 kV. Its working characteristics contain a region of negative differential resistance; increasing current up to 100 mA the voltage decreases at about 2 %. The power supply for magnetron and the directional coupler for the relative microwave power measurement were designed as well. Real power was measured according to calibration curve achieved from calorimetric measurements.

The coil should give magnetic field strength of at least 0.0875 T in region of cylindrical wave–guide. The calculation for the winding results its optimum shape 200x100 mm of the cross section. Water-cooling enables to choose the current density more than 5 A mm^{-2}. The combination choice of the wire cross-section and the number of turns is given by power supply. In order to keep the magnetic field strength constant independently on rising temperature of copper winding a current source is used again. The field strength of 0,0875 T in the center of the system axis at power 12.6 A/20 V was achieved and its movement along the axis with coil current variation is enabled.

1.2.3 Properties of plasma source

The micro–wave power introduction into plasma have limits given by adaptation of the system. So its correct measurement is dependent on immediate state of a load. A water load was used for calibration of power supplying the magnetron. Repeated measurements show that the efficiency of power transfer increases with power supplied into magnetron from 35% at 60 W to 45% at 300 W.

The basic parameters of the plasma source were measured mainly by using hydrogen as discharge media according to the purpose of the source. Plasma parameters were measured by using cylindrical Langmuir's probe on the axis at the distance 7.5 cm from the plasma source orifice – see Fig. 1.2. Measured probe data characteristics were processed according to Šícha [19]. The calculated values of energies and concentration concern to this point on the source axis according to impossibility of location probe into the discharge chamber Conditions for the discharge ignition in hydrogen are characterized by the severe minimum micro–wave power in the magnetic field strength dependence at ECR conditions. Considering the fact that ignition is initiated in ECR region; its probability depends on ECR region volume. In vacuum there is a plane of infinitively thin thickness, but practically we can consider the thickness limited by the electron mean free path component in direction opposite to field gradient. At the higher field the ECR region is moving down the coil axis and becomes thinner according to the higher field gradient and contains smaller volume of gas. So the ignition probability becomes lower.

It can be explained by presence of long–life high-energy metastable excited argon atoms and their larger effective collision cross–section. In case of hydrogen plasma density decreases below the pressure 0.1 Pa and below 0.05 Pa plasma damps. In case of argon the pressure for stable discharge can decrease down to 0.01 Pa. Electron energy only slightly depends on the microwave power but strongly on the pressure in agreement with the variation of the mean free path.

Plasma density depends on applied power as it can be seen in Fig. 1.3. The plasma density is limited by reflecting excess microwave power on plasma itself, for achievement of higher plasma densities much more power is necessary. The low plasma densities should be considered in connection with the probe location 7.5 cm out of the discharge chamber, where further plasma treatment of samples are expected.

The hydrogen incorporation into the a-Si:H growing film is qualified by the presence of excess dissociated hydrogen in the ambient atmosphere. Two fundamental processes in the hydrogen plasma were considered: generation accompanied by ionization, species excitation and dissociation and the second is the recombination of the species. The important parameter of hydrogen plasma is

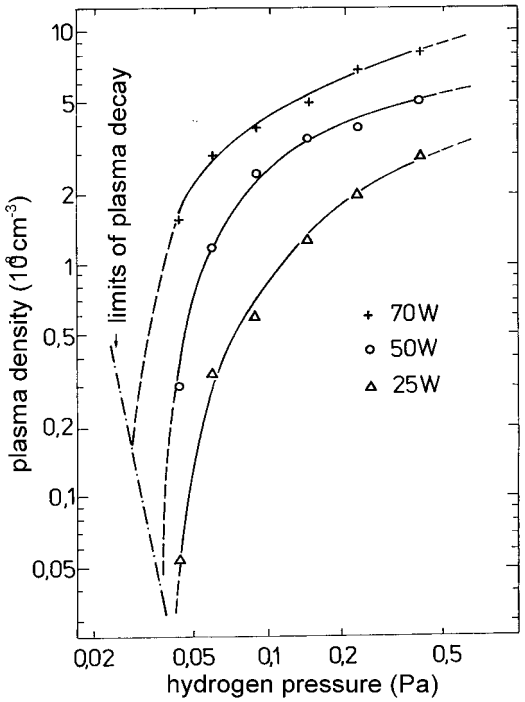

Fig. 1.3 Plasma density dependence on pressure for some applied powers and coil current 14 A in hydrogen

line of Balmer's series can be observed.

the degree of dissociation α. Using [20][21][22] the steady state concentration of dissociated hydrogen was calculated from equation:

$$n[H_2] = \frac{n_0}{\frac{4n_e QV}{\tau v_S A} + 1}. \qquad (1.4)$$

where initial concentration H_2, $n[H_2](t=0) = n_0$, n_e is the electron concentration and Q is the reaction parameter depending on the efficient cross section and electron energy distribution. At the dissociated hydrogen atom concentration $n[H]$, the mean atom velocity $v_s = \sqrt{(8kT/\pi m_H)}$ (k is the Boltzmann's constant, m_H is the hydrogen atom mass, T is the thermodynamic temperature, $T = 800$ K) N of hydrogen atoms impinge on the discharge chamber area A per the time unit. V is the discharge chamber volume and τ the recombination factor. For the approximate solution we achieved the dissociation degree α = 7 %. The direct measurement of the degree of dissociation was not carried out. The existence of dissociated hydrogen is confirmed from the spectral measurements, where a strong H_α

1.3 MICROWAVE MAGNETOACTIVE ION SOURCE

1.3.1 Physical background.

Ion guns were originally developed for reactive motors in space technology [23]. Later they were used in solid-state technology for ion beam treatment of surfaces, stripping, etching and secondary ion beam deposition instead of sputtering for thin film creation. It consists of a discharge chamber and a system of extraction grids for extraction, acceleration and deceleration of the ions. Former Kaufmann's proposal uses the electron source from the tungsten-heated cathode for gas ionization and external magnetic field to prolong the electron paths. Extraction grids can be applied also on some electrode–less low-pressure discharges. The condition, when the mean free path of extracted ions is much larger than the chamber dimensions, can be fulfilled using the magnetoactive discharges.

Two-grid extraction system for the MW ECR plasma source was developed for hydrogenation of amorphous silicon and some related techniques. According to the magnetic field strength in direction to the extraction system and diamagnetic nature of plasma, the electrons and ions prefer to be accelerated in extraction region. On the basis of Kaufmann's calculation of the ion source [5] an approximate power for required ion current can be calculated. In our case the primary ion region A_p is approximately equal to the inner surface of the discharge chamber, it means it is 250 cm^2. The area of extracting outlets is approximately 12.5 cm^2. It is presumed that the extracting voltage creates continuous extracting area (plasma boundary). The single outlets plasma boundaries join to the large extracting area equal to $A_{ex} = 12.5$ cm^2. Energy required for a single ion E = 1,000 eV and since that power 1 kW for 1 A of the ion current. Considering microwave power input 50 W we can expect the total ion current according to non perfect impedance matching the discharge chamber some tens mA.

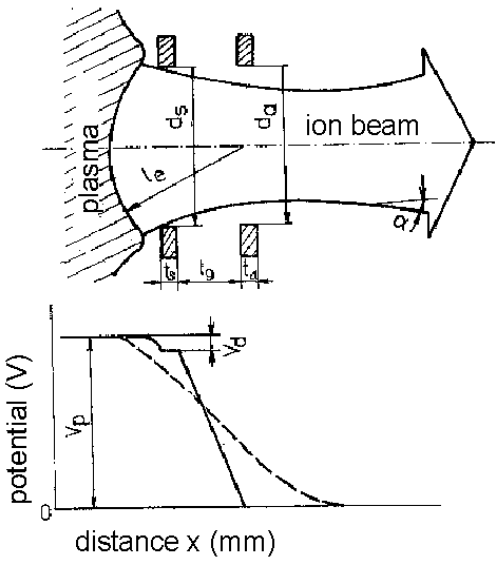

Fig. 1.5 The geometrical assembly of the ion source extracting system with the grounded acceleration grid. [5]. d_s, d_a – aperture diameters of the accelerating and screening grids, t_s, t_a – thickness of the accelerating and screening grids, l_e – effective accelerating distance (the field region), l_g – grids distance, V_p – plasma potential, V_d – potential drop on the screening grid, – – – potential decrease on the aperture axis, —— potential decrease on the axis of intergrid region, α – beam divergence

The molybdenum planar grids used for ion sources of beam diameter not exceeding 100 mm are in our case sufficient. The solution of Poisson's equation on the plasma boundary for zero field brings the ion beam current density. The total ion beam current through a single aperture is acquired by its multiplication of the area of the screen grid aperture.

$$I = (\pi\varepsilon_0 / 9)(2q/m)^{1/2}\left(V^{3/2} d_s^{\,2} / l^2\right), \tag{1.5}$$

where ε_0 is the electric constant, q and m are charge and mass of the ion, V is the potential difference between the plane of ions origin (plasma boundary) and plane of measuring, l is the distance of those two planes, d_s is the aperture diameter - see Fig. 1.5.

1.3.2 Ion source project

Using accelerating voltage 100 V and ratio $l_e/d_s = 0.5$ it is possible to extract current I = 25 μA through a single aperture, using 1,000 V we obtain 0.8 mA. According to larger perveancy for hydrogen the currents are six times larger. The beam divergence is between 10° and 15° and decreases with prolongation of the grid distance l_g. The optimal design of the two-grid extraction system is a compromise among several demands.

We choose $l_e/d_s = 1/3$; $d_s = 3.5$ mm and $l_g = 1$ mm. In order to prevent the capture of ions on the accelerating grids, the apertures of both grids should be severe coaxial. The designed grid system gives at the hydrogen discharge chamber pressure 1 Pa and extraction voltage 700 V the total beam current 50 mA.

We presume the molecular flow at considered pressure 1 Pa. The air aperture conductivity

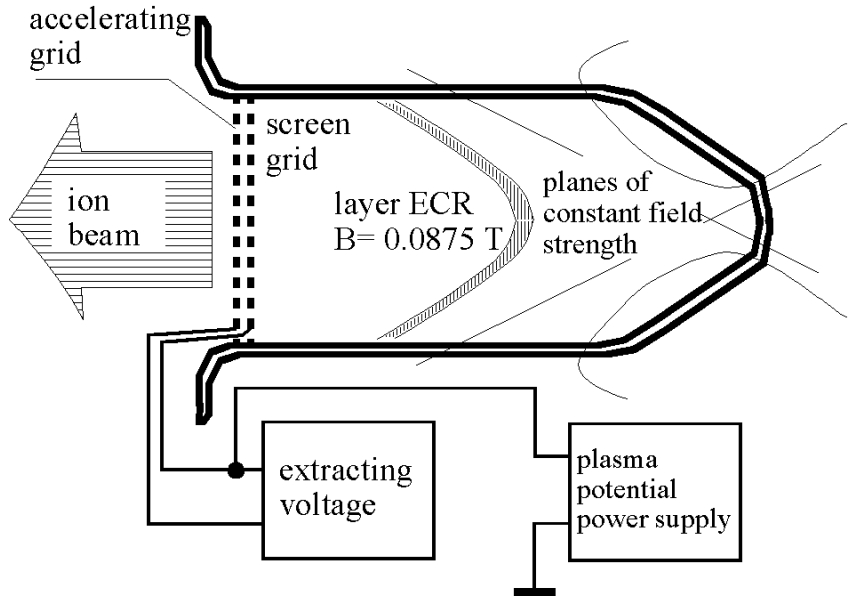

Fig. 1.4 Discharge chamber of microwave ECR plasma source with ion beam extraction system

of two coaxial apertures of the grid $G = 4.34 \cdot 10^{-7}$ m^{3}s^{-1} for air was calculated according to eq. (1.5) While the air-pumping rate is 1.3 m^{3}s^{-1}, the pressure in the discharge chamber is 1 Pa and 62 apertures is the recipient pressure 0.07 Pa. The grid conductivity A = 1.64 m^{3}s^{-1} and the pumping rate 1.64 m^{3}s^{-1}. While setting the hydrogen flow rate to processing conditions the pressure in the discharge chamber is about 0.7 Pa. During the discharge increases the gas temperature and also the species number rises because of dissociation. Its effect on chamber pressure is difficult to express.

The screening grids define the plasma potential according to the fact that no other electrodes are in the discharge chamber in contrast with Kaufmann's type ion sources.

The gas inlet is realized with the silica pipe 8 mm in diameter through the orifice in the periphery of the grids. The screening grid did not touch the pipe so no surface sparking could appear. Moreover the pipe is shielded so the ion extraction is not allowed along the pipe. Convenient for the extraction was the adjustable positive voltage power supply 1000 V/400 mA.

The extracting system with power supplies for extraction and plasma potential are depicted in Fig. 1.4. The divergence of the ion beam increases with the ion beam current because of the increase of space charge density and from the same reason it decreases with accelerating voltage growth. The ion beam divergence can be pushed by addition of electron emitter just behind the grid system. The positive space charge of the beam is neutralized by electrons and the repulsive forces extinct.

1.3.3 Verification of extracting system

The ion source properties were measured as the dependence of the total ion beam current on the extracting voltage and the pressure for hydrogen and argon. The V-A characteristic is in Fig. 1.6 resuming that the total ion beam current is a bit smaller by the subtraction of the accelerating grid current. There is evident decrease of the accelerating grid current at about 200 V. The theoretical value of the extracted Ar ion current for the grid system with 62 orifices at single orifice current is 0.8 mA, for hydrogen with 6 times larger perveancy than argon at extracting voltage 1000 V is 300 mA. Practically at plasma losses 100 W it was achieved the current 160 mA. This means, that an effective accelerating distance l_e according to achieved plasma density is still much larger than the grid distance l_g.

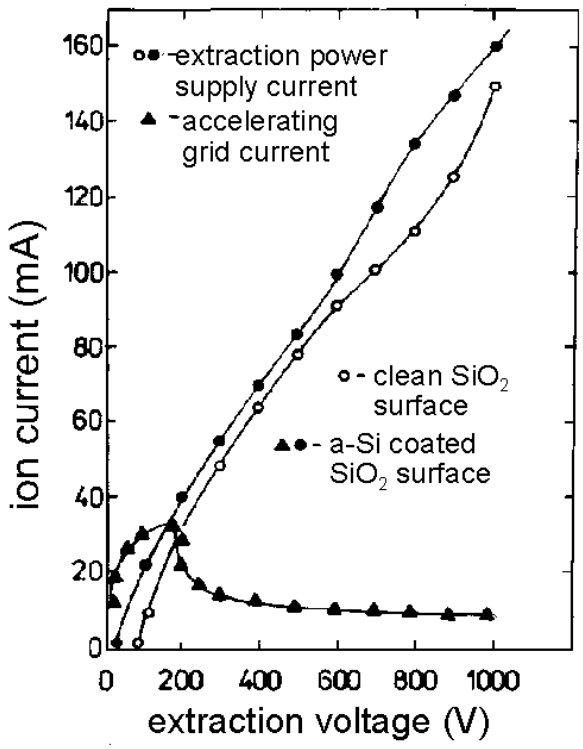

Fig. 1.6 The dependence of the power supply current on extracting voltage. Measured for discharge losses 100 W, hydrogen pressure in the discharge chamber 1 Pa. The total ion beam diameter is limited by an orifice of 40 mm in diameter in a front of the grid system

The ion beam current density measurement for some extracting voltages for argon and hydrogen was carried out with a moving Faraday's cup detector with an orifice of 2 mm^2 in cross section in the distance 120 mm from the accelerating grid without the neutralizing electron emitter. It is larger for hydrogen according to larger perveancy of hydrogen. In this arrangement it is possible to achieve the ion beam diameter from 40 to 60 mm (the FWHM value) with current density over 1 mA cm^{-2}. The hollow beam can be created at the accelerating voltage about 1000 V and plasma losses 100 W.

The total ion current at constant plasma density is proportional to the extracting voltage.

Since the equation of continuity should be fulfilled for the extracted current, the extracting voltage increase causes increase of the plane of ion origin – the plasma border defined also by the Debye's screening distance. This plane area is close to the area of the screening grid. In case of its diameter 40 mm^2 (area A = 12.5 cm^2), the number of ions going through the plane of ion origin at the total current I = 160 mA during the time 1 s is

$$v = I / A_i e = 8 \cdot 10^{16}\,\mathrm{s^{-1}cm^{-2}} \tag{1.6}$$

Resuming the mean ion energy in plasma 1 eV is their mean velocity $v_a = 10^6$ cm s^{-1}. The ion concentration in plasma, in case of quasineutrality also plasma density, is then

$$n = 4v / v_a = 3.2 \cdot 10^{11}\,\mathrm{cm^{-3}}\,. \tag{1.7}$$

This value is close to the critical plasma density for the 2.45 GHz plasma source ($n_k = 7 \cdot 10^{10}$ cm^{-3}). The hydrogen molecules concentration at pressure of 0.8 Pa and room temperature is $2.2 \cdot 10^{14}$cm^{-3}. The discharge ignition causes the temperature increase and simultaneously the vacuum conductivity of the grid increases. That leads to species concentration drop. On the other site the hydrogen dissociation causes the species number rise. The vacuum conductivity of the grid system for dissociated hydrogen is higher two times and it contributes to species concentration decrease. According to difficulties in discharge temperature determination the true species concentration can be only estimated to 10^{14}cm^{-3}. The degree of ionization is then 0.1 %.

The described extraction system was tested with argon and hydrogen. The processing ion beam current density was usually 1 mA cm^{-2} at the extraction voltage 1000 V. These conditions were set up while the simultaneous electron beam evaporation demanding pressure less than 0.1 Pa was running. So the extracting area was reduced to 12.5 cm^2. The full open area 50 cm^{-2} provided much larger currents more than 300 mA at extracting voltage 400 V. It was limited by the power supply shortage.

1.4 SILICON EVAPORATION

Silicon evaporation was promising method due to its relative simplicity and pro-cessing without hazardous gasses like silane, diborane and phosphine. But the results were not satisfying from the point of view DOS characteristics. Material shows usually poor photo-conductivity caused probably by increasing of density of so called tail states. The reason can be in condensation mechanism of silicon vapor. The condensed particle with multiple bonding electrons does not relax to release stress. It leads to creation network with inner strain and subsequently higher DOS in tail states. Weak photo–conductivity was achieved in case of low deposition rates in excess of surrounded dissociated hydrogen. Hydrogen affects as etching media for stress releasing. The excess of dissociated hydrogen with combination of low deposition rate and high substrate temperature can restrain the tail states, but moreover UHV deposition conditions are required to avoid oxygen incorporation. The preparation of a-Si:H of electronic grade quality by evaporation was published only rarely. Several remarkable results were published about hydrogen assisted EBE of silicon [24],[25],[26],[27] but they were not continued.

1.4.1 Electron gun

Convenient material for EBE of silicon is pure poly-crystalline silicon. Liquid silicon is very reactive, it dissolves all metals by creating silicides, and it creates carbide with graphite. Convenient for evaporating is only electron gun. Classic electron gun evaporator contains water-cooled copper crucible of some cm in diameter. In it molten silicon is unstable and causes explosion and splashing material inside vacuum chamber.

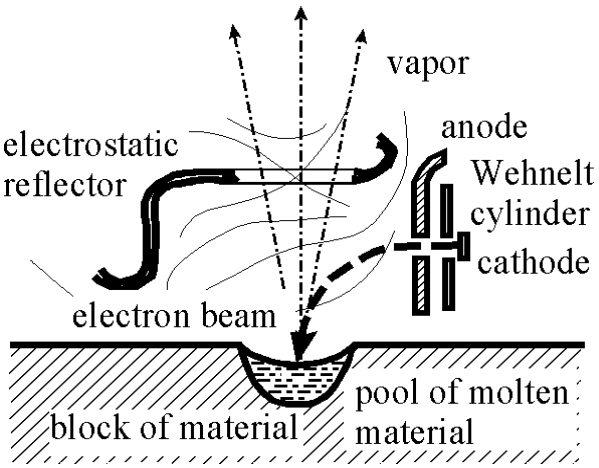

Fig. 1.7 Construction and function of electron gun evaporator

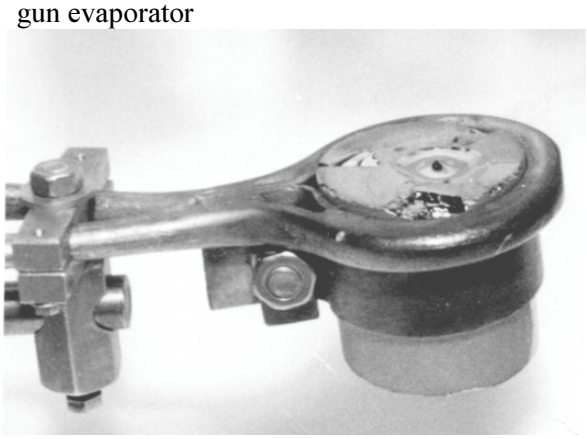

Fig. 1.8 Cooled ingot of polycrystalline silicon after electron beam evaporating from the top center

Optimal method is evaporating without a crucible. Only block of silicon – cylinder of about 100 mm in diameter and 100 mm high – surrounded by copper cooling pipe can be evaporated from a pool of molten material without a crucible. The principle is apparent from Fig. 1.7. Evaporation is stable for a long period limited by the cathode lifetime. When dumping the electron gun the molten material solidifies into the sharp tip in the center that resulted from silicon expansion. Eventual impurities concentrate into this tip; therefore simple breaking and removing can purify material –see Fig. 1.8. Also new material can be added easily.

Instead of magnet an electrostatic reflector of the cathode potential was used for electron beam bending – see Fig. 1.9. In that case the electron trajectory is independent on accelerating voltage so unfiltered DC voltage power supply of 10 kV/300 mA can be applied.

1.4.2 Silicon condensation and a-Si:H thin film growth.

With an exception of a technique ICBD (Ion Cluster Beam Deposition) [28], evaporation vapor consists of a beam of Si atoms. Si particles impinge on substrate and at the temperatures below 525°C there is their surface mobility small so amorphous network with number of dangling bonds is created. Presence of dissociated hydrogen in ambient space causes saturation of those dangling bonds. Molecular hydrogen behaves as an inert. Implantation of hydrogen ions of energy 5 keV causes deep precipitation of hydrogen and voids creation. Low energy ions affect etching in direction of their beam and typical surface texture. An excess of dissociated hydrogen causes its bonding in atomic concentration up to 40%. The concentration can be also controlled by substrate temperature. The resulting films are similar to those prepared by CVD techniques but occur only slight photoconductivity. The mechanism of thin film growth offers an explanation.

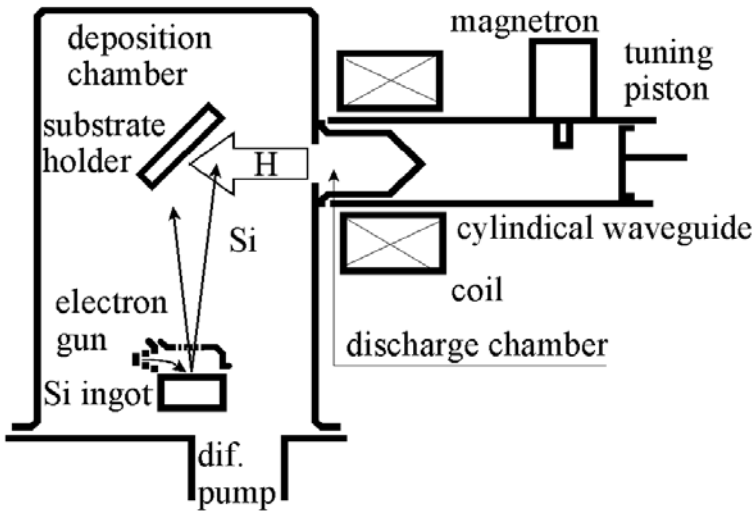

Fig. 1.9 Apparatus for hydrogen plasma assisted EBE of silicon

This method continued the ion beam assisted EBE a-Si:H preparation method based on RF discharge ion gun presented earlier [29].

1.5 MICROWAVE ELECTRON-CYCLOTRON-RESONANCE PLASMA-ENHANCED CHEMICAL-VAPOR-DEPOSITION (MW ECR PE CVD) METHOD

1.5.1 Description of apparatus for a-Si:H thin film deposition

The MW ECR plasma source was modified and applied on MW ECR PE CVD a-Si:H preparation [30]. The geometry, typical of ECR plasma processing chambers, is shown in Fig. 1.10. It consists of the MW ECR plasma source described in chap. 0 and a deposition chamber constructed as a stainless-steel vacuum chamber of 30 cm in diameter and 25 cm of height. The substrate holder of area 6×6 cm is located at a distance of about 8 cm from the end of the discharge tube. This copper holder can be heated by current flow through resistance wire up to 550 °C. Substrate temperature is monitored by thermocouple sealed in glass and by 100 Ω platinum thermometer placed inside the holder. Recently we have used a rotary type of substrate holder with 6 active deposition positions with area of 3×6 cm but then we were not able to ensure sufficient insulation from the deposition processes at just non-active positions. Moreover some problems have appeared during the depositions at high temperature (>300 °C) when substrate temperature in inactive positions increased more than 30 °C in comparison with active position. Nevertheless, more than 30 interesting deposition series were done with this geometrical configuration.

Plasma generation gas (H_2, Ar, He or their mixture) is fed through a stainless steel and ceramic inert tubes to the plasma chamber. Silane gas (SiH_4) is brought directly to the deposition chamber through a copper ring shower of 70 mm in diameter with 20 holes (of 1 mm in diameter) oriented towards the substrate holder. The gas supply manifold and pumping systems of the vessel is described in [30]. Each gas flows through several control valves and mass flow controller. In case of using mixture of plasma generation gases (He and Ar), they are at first mixed and subsequently enter the plasma CVD chamber. The possibility of doping by phosphine gas (PH_3) or diborane gas (B_2H_6) is also presented

The plasma-processing chamber is evacuated to the base pressure about 10^{-4} Pa. This pressure is kept more than eight hours before the deposition together with heated apparatus to enable desorption of residual gases. The pumping rate of the diffusion pump is reduced approximately 5÷20 times by a rotary shutter before starting plasma to attain the required pressure inside the deposition chamber. During the deposition the unreacted remnants of silane and hydrogen are burned in a gas flame burner and washed away by a water jet.

We have tested four geometrical deposition systems including standard configuration described above. The first modification consisted in location and orientation of the substrate holder to the wave-guide axis (parallel to it). By this modification we have attempted to eliminate bombardment of the growing surface by all active particles originating from plasma. Some physical properties of deposited films have been indeed improved, mainly concentration of hydrogen atoms bonded as dihydrides was severely reduced. On the other hand deposition rate decreased about 5 times in comparison with a standard deposition configuration and moreover homogeneity of film properties in the first order homogeneity of film thickness got worse.

The second was led by the aim to prevent the penetration of SiH_x molecules and radicals into the plasma chamber. We have placed a grounded grid (from stainless steel wires of 0.15 mm in diameter with period of 0.6 mm) between the plasma chamber and the reaction chamber. A deposition rate rapidly decreased and moreover, some thickness fluctuations in the film have appeared with period of about twice of the period of the wire grid. In agreement with [31], this fluctuation corresponds well with the distribution of the electron flux on the growing surface. This is explained by the observation that the electrons produced in the ECR plasma move along the magnetic field lines and play a key role in the dissociation of a source namely on the growing surface of the film. It may be possible that the electrons do not have energy high enough to dissociate the adsorbed SiH_4 molecules and to occupy optimal bonding configuration. This might

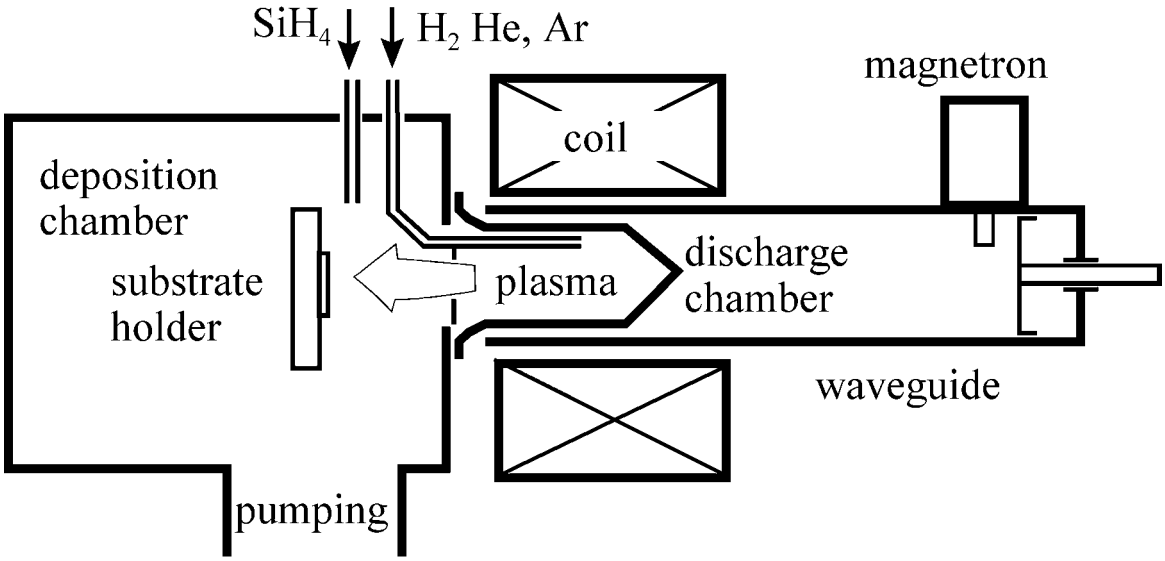

Fig. 1.10 Microwave Electron-Cyclotron-Resonance plasma processing chamber

be the reason for high hydrogen concentration in films prepared by MW ECR PE CVD at low pressure, mainly in SiH_2 and $(SiH_2)_n$ chain configurations.

The total energy transferred to the film surface depends on the ion density and the kinetic energy of ions accelerated by the electric field in an ion sheath, which are enhanced by increasing the microwave power, reduced pressure and applying a negative DC bias with respect to the surface. The best results in all laboratories (in a fact by suppression of SiH_2 concentration) were achieved with negative DC bias voltage. The secondary effect of the negative DC bias voltage is the blocking of the electron bombardment and just this blocking could be another reason for better film properties.

Our last "geometrical" modification consisted in the use of a plasma extraction source (an ion gun) for dissociation of SiH_4 molecules, i.e., by plasma without electrons in the deposition chamber. In this case energy of extracted ions can be controlled by voltage of the extracting grids in this system. We have expected quite different physical properties of the so grown layers but unfortunately silane flowing to the deposition chamber did not decompose almost at all and so the deposition rate was drastically reduced to the value below 0.01 nm s^{-1}. This experiment provided a quite clear evidence for the affirmation that the silane in microwave plasma is decomposed due to the collisions with electrons and not with the other energetic particles from plasma. These energetic particles such as ions and radicals can play an important role during the growth processes for capturing an optimal bonding configuration on the surface. Nevertheless, just this extraction system was further applied with success to the study of influence of the impinging electrons on the growing surface. In the case of the opposite electric field in the space between the extraction grids this system can be applied for choosing electrons (or negative ions) from charged particles in plasma. Details about the film properties are commented in [30].

2 THERMAL DESORPTION SPECTROSCOPY

2.1 INTRODUCTION

Thermal desorption spectroscopy (TDS) is based on mass spectroscopy of gases evolved from solids when they are annealed. It can be used for determination of the bonding energy of an evolved gas component and afterwards from that derive chemistry and structure of investigated material. This method was developed for amorphous hydrogenated silicon research and it was also used for silicon based polymers examination.

In case of amorphous hydrogenated silicon we consider only hydrogen as a single gas reaction product. The published methods were based on the thermo-gravimetry, mass spectroscopy [32] and gas chromatography [33]. According to the last reference the apparatus was developed in cooperation with the Institute of Analytical Chemistry CAS with good sensitivity [29]. In a laboratory of vacuum technology and thin films deposition using the mass spectroscopy seemed to be the most convenient method. The analyzed amount is usually very small depending on thin film thickness below 1 μm and its mass is of order μg. In order to obtain the benefit using this method it is important to verify it on well-defined materials disposing appropriate theory.

2.1.1 Theory

The theory of an interphase reaction is described e.g. in [34]. When a reaction in selected material runs in the way that one product is permanently removed by constant rate and is far from equilibrium, its concentration, (in case of gas we use partial pressure p_i,) depends only on the reaction rate r. Such conditions can be fulfilled in vacuum. Presuming the simplest case of the first order reaction and considering the arbitrary concentration (molar, mass or volume) of compound component C_i reaction rate is

$$p(t) = -\frac{\mathrm{d}C_i(t)}{\mathrm{d}t} = A\,\mathrm{e}^{-\frac{E_a}{RT}} \int_t^{\infty} p(t)\,\mathrm{d}t\,, \tag{2.1}$$

where E_a is the activation energy, R the molar gas constant, A the pre-exponential factor, T is the thermodynamic temperature and t is time

The integral on the right side expresses remaining concentration of a component i in the sample in time t. All constants are included into the pre-exponential factor A and instead infinity time we use the time of the non-detectable partial pressure when the precursor i is exhausted. The equation (7.3) is convenient for the activation energy E_a calculation.

In case a linear temperature sweep rate θ

$$T = T_0 + \theta t \quad \text{and} \quad \mathrm{d}T = \theta \mathrm{d}t \tag{2.2}$$

we can transfer equation (7.2) to temperature as the variable dependence

$$p(T) = -\frac{\mathrm{d}C_i(t)}{\mathrm{d}t} = A'\,\mathrm{e}^{-\frac{E_a'}{kT}} \int_T^{T_{max}} p(T)\,\mathrm{d}T, \tag{2.3}$$

where k is the Boltzmann's constant and E_a' is the activation energy per a single bond and it can be expressed in electronvolts.

The upper limit T_{max} expresses the temperature, at which the desorbed component is exhausted and T is the actual temperature. The temperature sweep rate is involved in the pre-exponential factor and it has no influence on the activation energy, which can be easily calculated. The model calculation is compared with both literature and experiment.

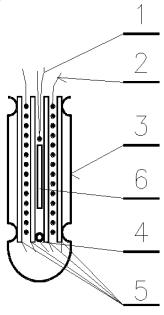

Fig. 2.1 Sample holder: 1- iron-constantan thermocouple, 2 - heated winding, 3 - shielding Mo sheet, 4 - corundum distance rod, 5 - corundum plates

2.1.2 Apparatus description

The apparatus was based on high vacuum apparatus AV63 (Tesla) and the quadrupole mass spectrometer Quadrex 200. The principal schema is on Fig. 2.2. The chamber 2 pumped by the diffusion pump 4 is equipped with the quadrupole spectrometer head 1. The sample is placed in the holder 9 separated from the chamber with mass spectrometer 2 by a

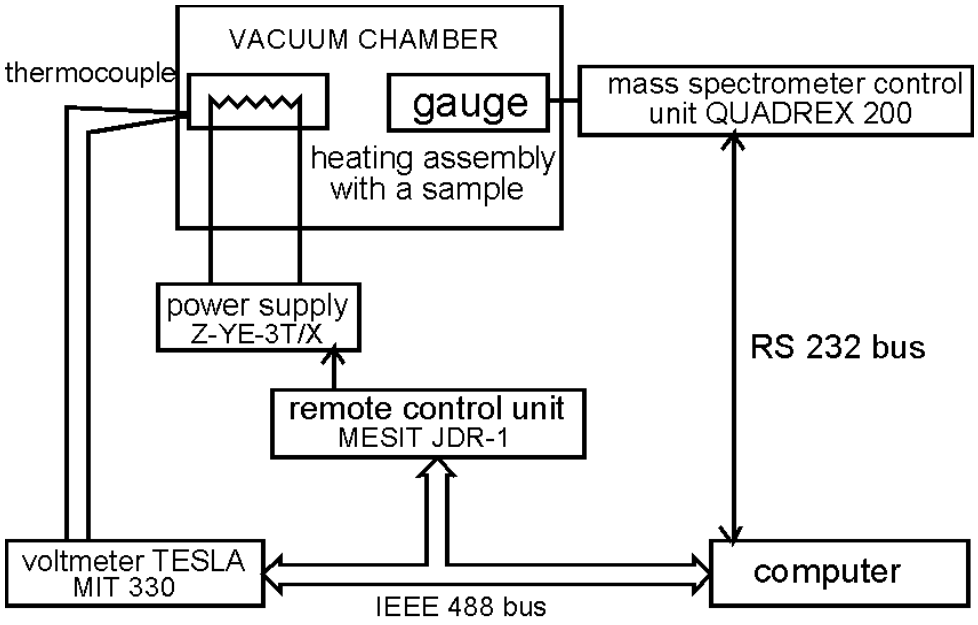

Fig. 2.2 Block diagram of the apparatus for temperature control and data acquisition of the thermal desorption spectroscopy (TDS) method

valve 3. It enables to change samples without vacuum breaking in analytic chamber 2 and shorten the pumping cycle. Detail construction of the sample holder connected to the temperature controller is in Fig. 2.1. It is constructed in order to keep its thermal inertia minimal and to keep also the controller time constant minimal. Heating power is minimized for reducing the thermal desorption from the chamber walls. It was constructed of thin corundum rods 4, plates 5 and thin molybdenum sheet 3 without any cement so its gas evolution was also reduced, even when heated on 700°C by the power 24 W. The sample 6 with thermocouple 1 was placed into the thin slit between heated corundum plates 5.

The dozer was made from calibrated burette. It enables to inject in the volume of needle valve reproducible amount of gas (8.0 μl). Calibrating was also carried out by injecting gas through the rubber septum by a micro-injector and the results were similar.

According to the pumping rate dependence of the diffusion pump on pressure for gas the dependence of integrating area of the partial pressure vs time plot was verified. The measuring apparatus is controlled by a computer see Fig. 2.2. The computer temperature control actuates the D/A unit with power output (Mesit Z-YE-3T/X), the temperature of the sample is measured by the iron-constantan thermocouple and the A/D converter (Tesla M1T 330) forming feedback for the control loop. All these instruments are connected to the computer by the IEEE 488 bus. The mass spectrometer Quadrex 200 is connected to the computer by the RS 232 bus. The Quadrex 200 enables to collect simultaneously values of 6 chosen adjustable mass numbers. The computer gives their time evolution on the screen display in both graphical and numerical forms.

The sample is inserted into the desorption chamber, pumped to the base pressure of 10^{-4} Pa, and after that the temperature starts to rise forming a linear temperature ramp. The hydrogen is evolved gradually expressing several typical peaks. After completing the desorption cycle at about 700 °C the calibration dose of molecular hydrogen is injected into the desorption chamber, while the data collection continues. The resulting data are then plotted against the time, integrated and calibrated for absolute and relative content calculation in atomic %.

An advanced apparatus for desorption analysis was built later and was based on ultrahigh vacuum chamber (see–Fig. 2.3). The system was developed in our laboratory and fabricated in the firm Vacuum Prague. The system is pumped by the turbo-molecular pump of pumping rate 150 l s^{-1} and the rotary pump of 5 m^3h^{-1}. Calibration is enabled due to a sapphire seat valve on the

side flange (not seen in the figure). The chamber is separated from the pumping unit by a gate valve of 100 mm in diameter. The chamber can be connected to another vacuum apparatus by a bellow tubing and connection DN 40 ISO KF for gas analysis in various other chambers and plasma reactors. The pressure drop is achieved by a changeable diaphragm.

The theory was verified on model of calcite thermal decomposition with good agreement and on aragonite powder – see Fig. 2.4. The result is compared by the differential scanning calorimetry (DSC) and thermogravimetry [35].

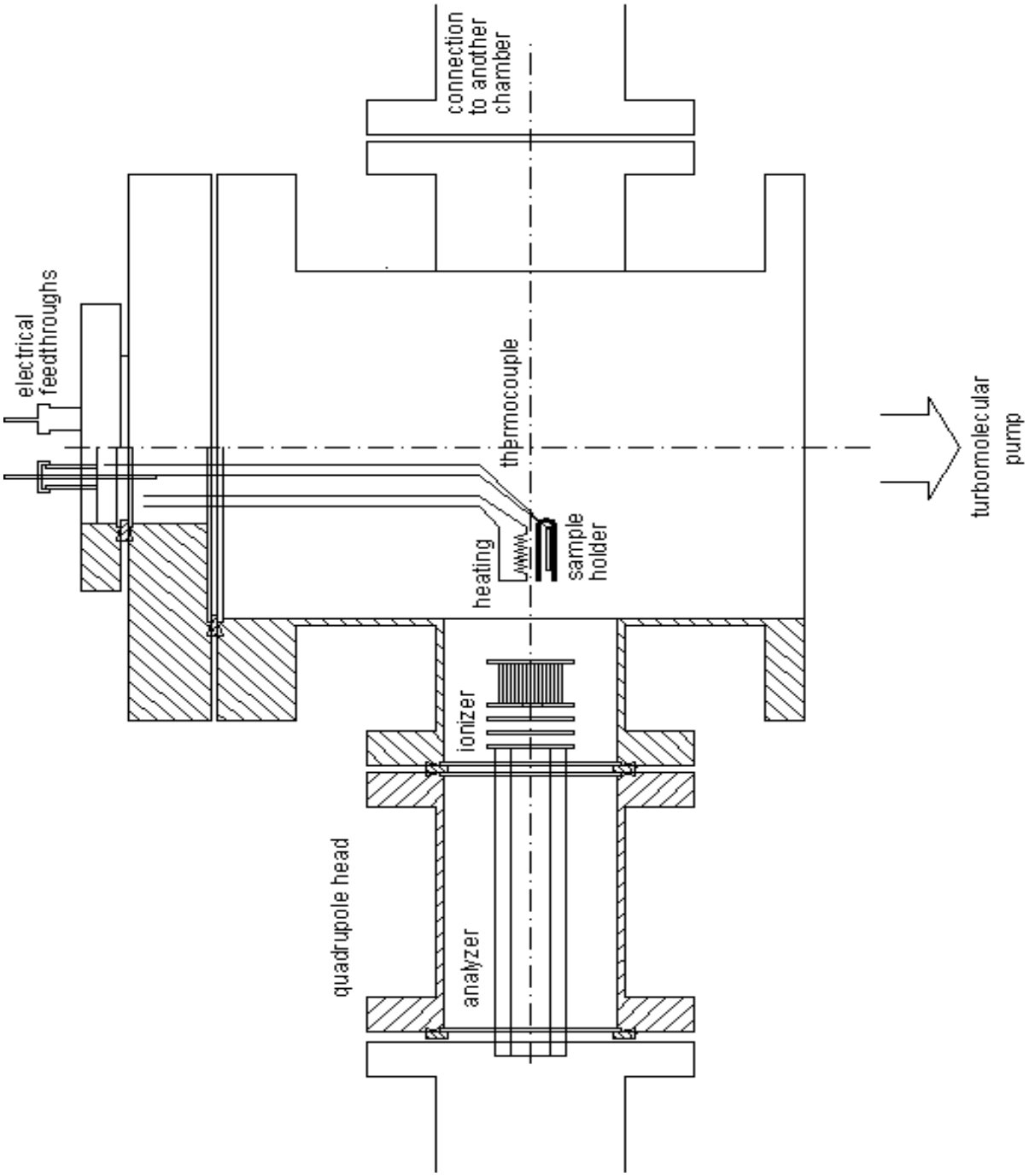

Fig. 2.3 Ultrahigh vacuum chamber for mass spectroscopy of thermaly desorbed gases

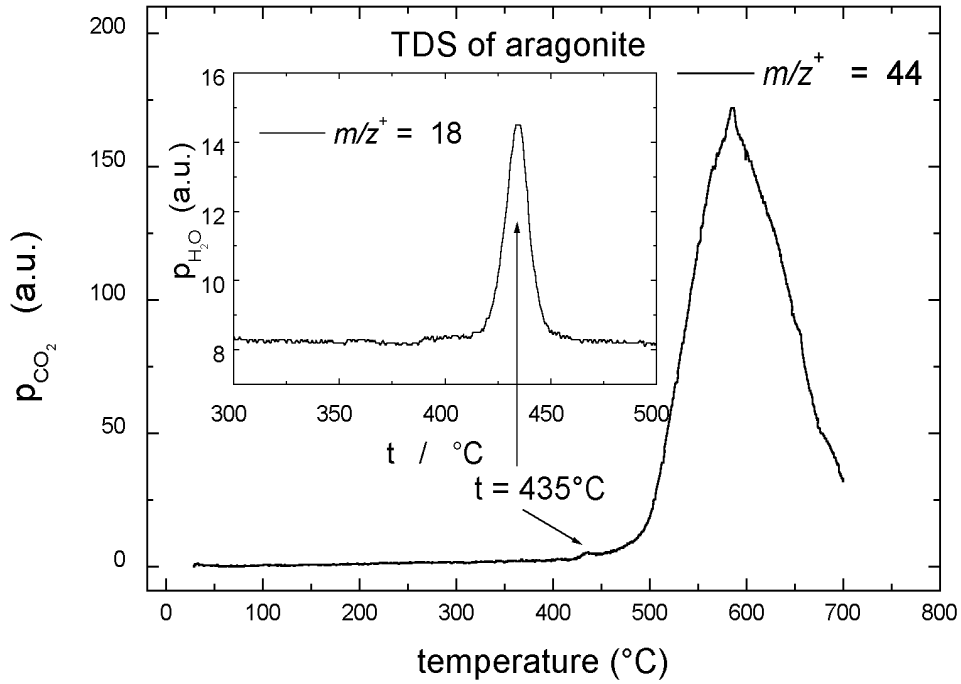

Fig. 2.4 Thermodesorption of CO_2 and water from aragonite

The temperature sweep rate influence was verified on thin films of plasma-polymerized dichlor-methyl-phenyl-silane. The samples were prepared on Si wafers. One evolved and detected gas component was hydrogen. For materials of films 1 cm^2 of area and 1 μm thick is convenient θ = 20°C min^{-1} and this option was mostly used in experiments. Fitting of function (7.3) on measured data for θ = 20°C min^{-1} gives E_a=91 kJ mol^{-1} = 0.94 eV per bond. Fig. 2.5 show the temperature dependence of the evolution curves, where the maximum shift is apparent.

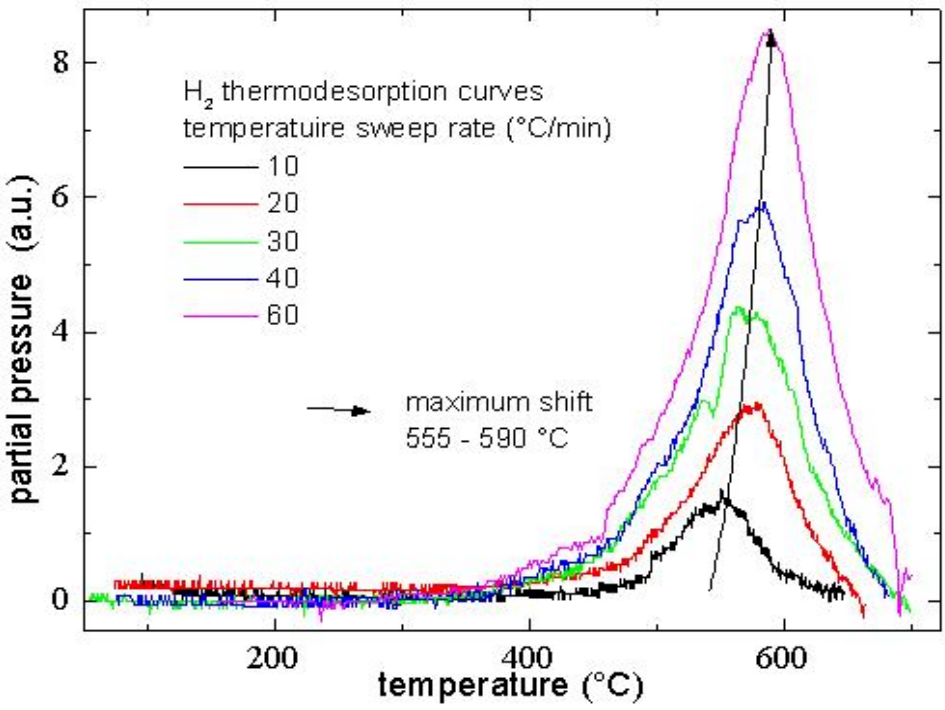

Fig. 2.5 Thermodesorption curves of hydrogen for various temperature sweep rates

2.1.3 Application on amorphous silicon

Amorphous hydrogenated silicon contains several percent of hydrogen, which influences its main properties such as radiation, absorption and density of states in the mobility gap [36]. Its content and bonding status is provided from IR absorption spectra measurement [37]. They also allow determining structure of the material, as columnar structure, existence of voids and other defects, which are described in chap.1.1.
Hydrogen concentration can be cal-culated by comparing integration area of desorption curve A_D with integration area of calibration dose curve A_C

$$C_H = \frac{1}{V_S}\frac{A_D}{A_C}\frac{V_{H_2}}{V_M}\frac{2N_A}{n_{Si}+n_H}, \tag{2.4}$$

where V_S is the sample volume, V_{H2} is the hydrogen calibration dose volume, V_M is the molar volume 22.4 l and N_A is the Avogadro's number.

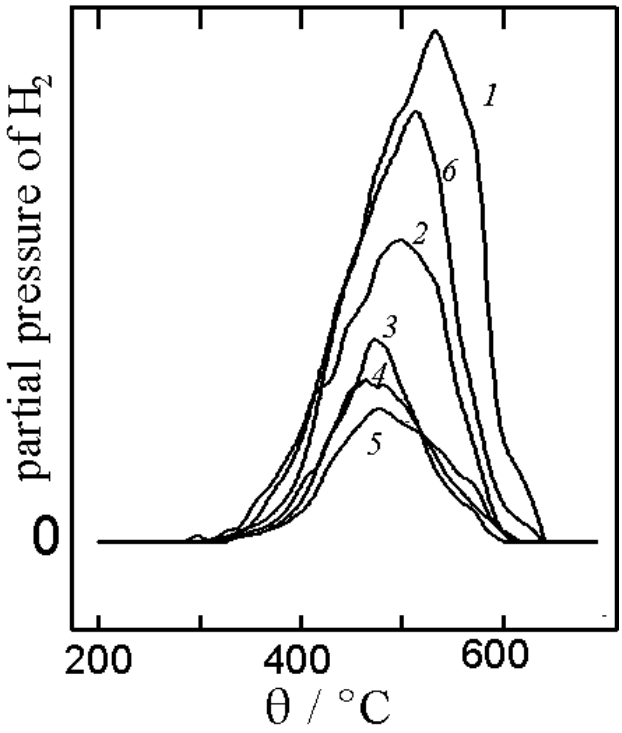

Fig. 2.6 Evolution spectra of RF power series of GD a-SiH

The method was applied on series of GD a-Si:H prepared in Institute of Physics CAS [38] and the results were published in [30]. The measurement preferred finding the total concentration of hydrogen in the material and not its binding energy. The evolution curves are in Fig. 2.6 and represent a series of hydrogen evolution from samples prepared by decomposition of silane in glow discharge at various RF powers. The total hydrogen content increases from 5 to 15 % with increasing power and is in good agreement with results achieved from IR spectroscopy measurements.

Other preparation methods of a-Si:H bring different TDS spectra although the IR spectroscopy show barely remarkable changes. A series of a-Si:H samples was prepared by microwave ECR CVD (described in chap. 1.6) and tested both by IR spectroscopy and TDS [39]. The examples of the results are in Fig. 2.7. The structure of the material according to chap. 1.1 plays an important role in TDS spectra but the IR spectra reflect only chemical bonding and its variation with the structure is negligible. The low temperature evolution peaks are connected mainly with decomposition of -SiH_2 which appear in the IR spectra a shoulder of 2 100 cm^{-1} close to 2 000 cm^{-1} peak. But low temperature evolution can be connected also with porous and columnar structure, not necessary with two hydrogen atoms bonded on one silicon atom.

Amorphous hydrogenated silicon (a-Si:H) films have been fabricated also by microwave plasma under high dilution silane SiH_4 with helium He. These films have been prepared to obtain a wide-band-gap (>2.0 eV) hydrogenated amorphous silicon that can exhibit visible photo-luminescence. The He dilution leads to the extension of the band gap because of the increase of the SiH_2 and $(SiH_2)_n$ configuration in the films. Absorption spectra in infrared (IR) and visible regions and photoluminescence (PL) spectra of these wide-gap amorphous silicon films are investigated and correlated with the deposition conditions [30][40].

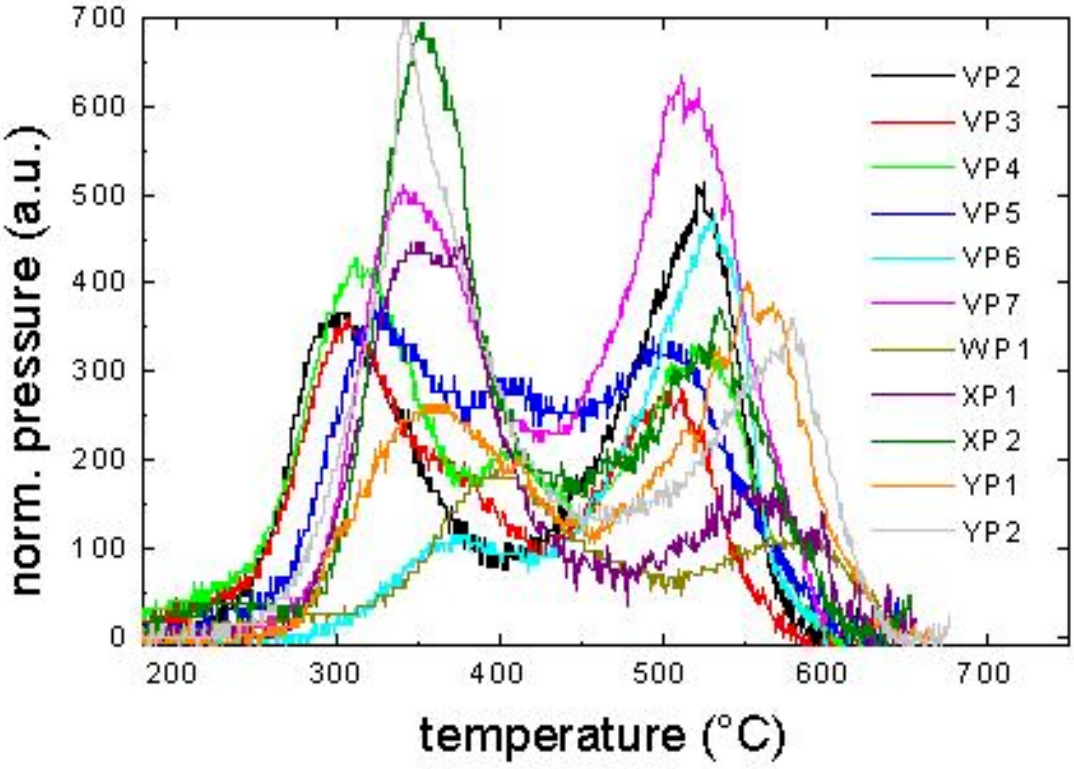

Fig. 2.7 Normalized TDS spectra of PL samples showing two significant peaks at temperature 350°C and 500-550°C

A series of such prepared samples exhibit two mean peaks, which can be processed separately and the activation energy according to model equation can be determined. The results are in Fig. 2.7. The high temperature peak is presumed to be controlled by decomposition of a-Si:H, when the reminder of hydrogen is evolved from the bulk. The diffusion of hydrogen to the surface has a negligible effect according to existence of the evolution at much lower temperature, where it can be controlled by diffusion. The reaction order n is closed to 1 according to a presumption and the activation energy E_a=1.64 eV is expected. The precision of the method is influenced by the noise

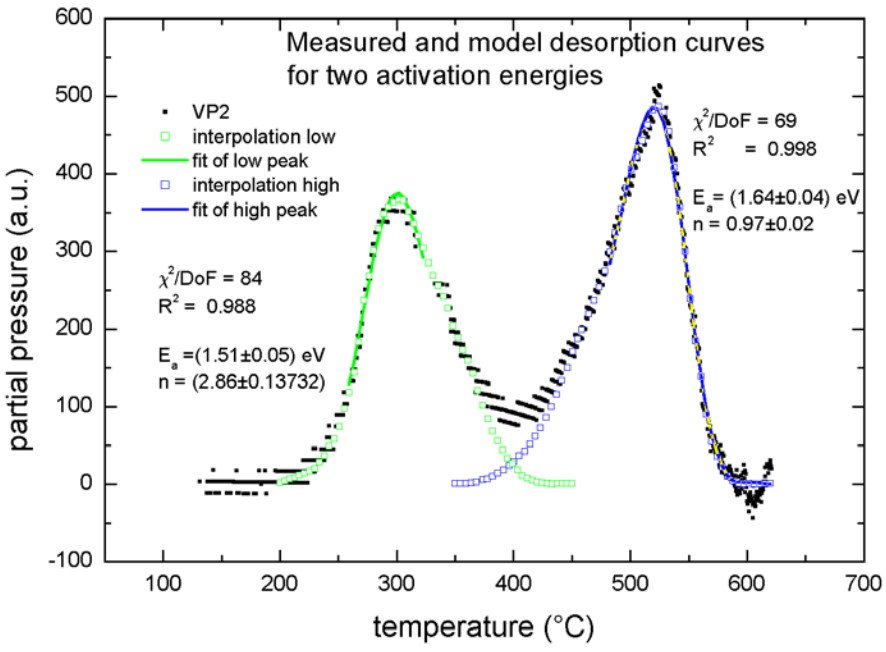

Fig. 2.8 Measured evolution curve, interpolated in two parts and fitted model

apparent from the measured curve VP2 and is estimated at least 0.2 eV. The fitting calculus gives an error for interpolated curve fitting and it is limited by the fitted region. The E_a parameter set in the vicinity of the calculated value ±0.2 eV gives also a satisfying fit and n value. The carefully estimated error is ±20%.

The different situation is in case of processing the low peak data. The same model gives values in the figure description. The value of n is unusual, so the model is presumed not to be correct for this region. The more common expression should be taken in account.

$$\frac{\mathrm{d}a}{\mathrm{d}t} = A\,\mathrm{e}^{-\frac{E_a}{RT}}\,\mathrm{f}(a)\,. \tag{2.5}$$

The hydrogen evolution is likely controlled by the diffusion process and the reaction mechanism on the inner surfaces in porous material can be miscellaneous. The total evolution curve is likely composed from other peaks like that in Fig. 2.8, which can influence the calculus, but they can be hardly distinguished.

3 POLYSILYLENES

3.1 GENERAL PROPERTIES

Polysilanes have many interesting properties for electronic applications, therefore they are widely examined in various applications, especially in OLED (Organic Light-Emitting Diode) structures. This group of substances can be described by a simple formula depicted on Fig. 3.1.

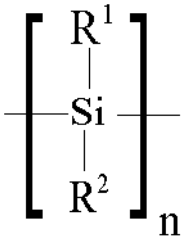

Fig. 3.1 General formula of polysilylenes, R1 or R2 alkyl or aryl group

Various technologies can be used for the thin films preparation: spin coating, casting, vacuum evaporation, plasma deposition, and Langmuir–Blodgett (LB) technique. The present research work concerns the deposition of poly(methylphenylsilylene) (PMPS) films mainly by evaporation techniques and their comparison with classically deposited polymers and plasma deposited polymers. The aim of the work is to find material for the large area light-emitting displays operating in general at low drive voltages and also the physics behind this deposition process. Several aspects dominate the research activities: deposition of films on various substrates, film analysis, characterization of the deposition conditions and their influence on the deposition process.

Polysilylenes as one of large class of silicon backbone solids including amorphous silicon are of considerable interest because of their unusual electrical, photoelectronic and non-linear optical properties. This exhibits because of its electronic structure - the easy delocalization of the σ-bond electron along the silicon chain [41]. The bond is introduced through interacting $3sp^3$ hybrid orbitals. The resonance integral between two orbitals located in adjacent silicon atoms and

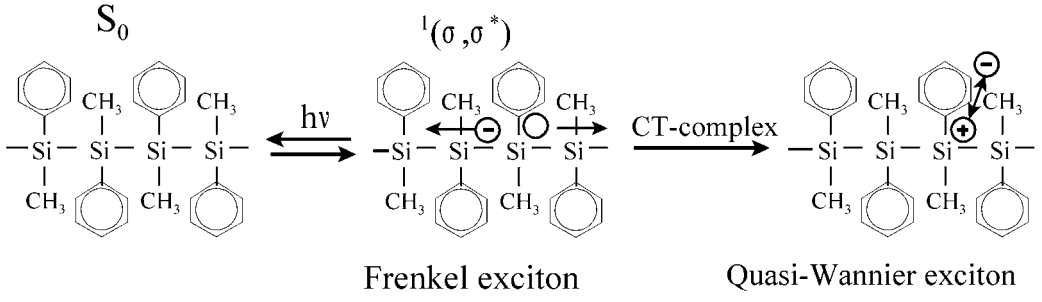

Fig. 3.2 Creation of Frenkel exciton $^1(\sigma,\sigma^*)$ and consequent capture of the electron on the side phenyl group – quazi-Wannier exciton

pointing to each other, β_{vic}, is responsible for the formation of the Si–Si* σ-bond.

Thin polysilylene films exhibit remarkable absorption and luminescence in the near UV region resulting from σ-electron delocalization along the silicon backbone. The molecular chain can be considered as a quantum wire, where the holes can move and recombine with the electrons in radiative centers. Polysilanes seem to be good charge carrier transport materials with high light emission efficiency and can be used for fabrication of electroluminescent diodes with light emission from the ultraviolet to visible region. By using double injection contacts, one can construct efficient electroluminescent devices where the recombination occurs near the interface between the polymer and the electron-injecting electrode.

3.1.1 Preparation of polysilylenes

The synthesis of polysilylenes with high degree of control is still rare, though there are successful methods in organic chemistry. Most polysilylenes are still synthesized by the sodium mediated condensation of the corresponding dichlorodiorganosilanes in n inert solvent using the Wurtz-type reductive coupling reaction [42][43].

Resulting polymer should be prepared in thin film for testing electrical and optical properties. Polysilylenes are usually soluble in toluene of tetrahydrofurane and other organic solvents. The solution can be coated on the substrates by casting or spin coating. Simple poly(dialkylsilylenes) have poor solubility. The non-solubility predestinates it for the alternative preparation methods, especially evaporation of the polymer. Poly(dimethylsilylene) PDMSi, is not practically soluble. Its simplicity both by availability of original material for the synthesis and physical interpretation of measured properties predestinate it for the fabrication of the luminescent devices. Its emission wavelength is 325 nm and it is the shortest of all materials from the group of polysilylenes.

Poly(alkyl-arylsilylene)s and poly(diarylsilylene)s are well soluble. The widely spread representative of this group is poly(methylphenylsilylene) - PMPSi. They differ by a slightly polar phenyl groups that behave like acceptors. The phenyl side group stabilizes the chain and serves as an electron trap.

Polysilylenes chain, with methyl or phenyl group on each silicon atom, behaves as one-dimensional system with weak intermolecular interaction. Features of the material are reflected in the energy diagram of electron state. At least two or three main absorption bands are detected in solid polysilylene films.

3.1.2 PMPSi thin films properties.

PMPSi is created from linear chains. The single unit molecular weight is105. The chain is bonded by σ electrons that can be delocalized. The possible electronic transfers cause photon absorption and electron transition into the σ* state at the range of photon wavelengths of 300-400 nm and in addition ππ* absorption on the phenyl group. The index of refraction is about 1.5, energy band gap E_g = 4.65 eV. PMPSi is usually described as an amorphous polymer. The chain breaking and evaporation is evident at 340°C.

The electronic properties can be best explained on the band model. The σ-σ* transition products exciton, that can be decomposed by the electric field to electron - hole couple. The electron is trapped on the phenyl group, but the hole localized at the backbone can thermalize and move in electric field. The polysilylenes occur photoconductivity under UV radiation which can raise σ-σ* transition and in addition π-π* absorption is observed. The energy of the σ-σ* transition moves to the lower value by overlapping of σ and π orbitals. (In case of polydialkylsilylenes the absorption λ_{max} = 300 - 320 nm, polyalkyl-aryl silylenes λ_{max} = 337 - 350 nm, poly-diaryl silylenes λ_{max} = 400 nm).

The vacuum deposition is an alternative method of epitaxial growth of oriented thin films and provides possibility to fabricate multilayer devices in les steps. The plasma-enhanced chemical-vapor–deposition (PE CVD) method enables to create the thin film directly from the original monomer. Both of these methods were tested and thin films were investigated in our laboratory.

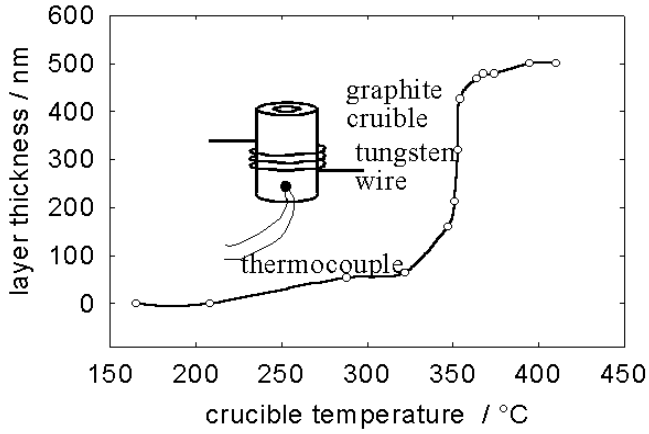

Fig. 3.3 Dependence of layer thickness on crucible temperature during deposition

The materials prepared by various techniques differ by their conjugated lengths. At a spin coated sample, where the conjugated length is large, significant σ-σ* transition and π-π* absorption is observable. At an evaporated sample the conjugated length is shorter and weak σ-σ* transition and π-π* absorption occurs. At plasma deposited cross-linked sample is no observable σ-σ* transition and only band absorption and weak π-π* absorption.

3.2 EVAPORATED FILMS OF PMPSI

In case of non-soluble polysilylenes as e.g. poly(di-*n*-alkyl)silylenes, vacuum evaporation is preferred [44]. The other possibility for unconventional preparation from a corresponding monomer [45] is plasma polymerization. The last two techniques were investigated for the preparation of thin films of prototypical polysilylene poly(methyl-phenyl) silylene (PMPSi) in the present work and properties were compared with those of spin coated samples [46][47].

The structural orientation of the deposited film depends on evaporation conditions, such as the substrate deposition temperature, the deposition rate and the substrate surface structure. The temperature influences the macromolecular orientation, which is random in case of the substrates cooled to low temperatures (-150 °C) [44] and perpendicular to the substrate at room and higher temperature. UV dichroism is an effect used for testing the structure. It is more evident in the polarized ray. No absorption occurs when the electric field strength orientation is perpendicular to the molecular chain, even at the oblique beam incidence. However, it does occur at presence of the field strength parallel to the molecular chain direction. The influence of deposition rate was observed by Takeuchi and Furukawa [48].

3.2.1 Preparation of PMPSi thin film

In this study, vacuum evaporation was adopted to form thin films of PMPSi. The PMPSi powder was evaporated from the graphite crucible heated by the tungsten wire – see Fig. 3.3. The evaporation temperature and the film thickness were monitored simultaneously by a thermocouple contacted to the crucible and a quartz crystal thickness monitor respectively. It is supposed that the polymer decomposes to fragments of molecular weight 10^3 according to Kim and Matyjaszewski [47].

Thermal Desorption Analysis (TDA) of the evaporated films confirms fact that no fragments of mass number below 200 were observed by the mass spectroscopy. The film does not decompose, but it is simply reevaporated and condensed on cold walls and does not impact into ionizer of the mass spectrometer. The gas chromatography of the film confirmed existence of only three components identified like mono-, di- and three- monomer units compound. The more heavy species were below the equipment sensitivity.

Fragments impinging on the substrate condensate, but their fuzzy spatial structure makes their accommodation difficult. The longer chains partly reconstruct on the substrate. This is demonstrated by the shift of optical absorption edge to shorter wavelengths, and its decreasing slope caused by the enhancement of the molecular weight. It was found that both these parameters were strongly dependent on the substrate temperature during deposition. The layers prepared on substrates at low temperature (below 50°C) create continuous uniform structure. The films prepared at higher substrate temperatures exhibited an island structure with contact angle of 15°.

The fragmented molecules exhibited poor adhesion to a flat surface and so many attempts to increase the wettability of the films were undertaken. Only plasma-activated surfaces exhibiting satisfactory adhesion resulted in continuous films. The films were soft and consisted of low molecular weight materials, and some cross-linking via – CH_2- bridges occurred.

3.2.2 IR absorption spectra

IR absorption spectra were measured on FT-IR spectrometer NICOLET IMPACT 400. Infrared spectra can inform about the structure and composition of the polymer layers. The IR spectra allow distinguishing the oxygen incorporation into the films. The low deposition rate (<1 nm min^{-1}) influences also the network creation and incorporation of oxygen. It can be derived from comparison of the spin coated and evaporated sample IR spectra (see Fig. 3.4). Low deposition rate and air plasma after-treatment causes 1040 cm^{-1} peak evolution but the dominant effect is from the deposition rate. The cross-linking is concluded from appearance of the 1257 cm^{-1} IR absorption predicating to methylene bridges Si–CH_2–Si. The peak 1098 cm^{-1} is assumed to belong Si-Ph vibrations and its shoulder on 1120 cm^{-1} can be derived for the phenyl bridges at crosslinking, as it does not occur at spin-coated samples.

The condensation of polymer free radicals results in mechanically instable films. Satisfying results can be reached with low temperature substrates and discharge treatment following the deposition that stabilizes the films. The comparison of IR spectra of stabilized and not stabilized PMPSi thin film is evident from 1040 cm^{-1} absorption region of Si-O-Si but branching via Si-CH_2-Si groups is not evident. In case of hydrogen plasma treatment no 1040 cm^{-1} absorption peak evolution was observed. The post treatment changes are not observable in IR spectroscopy.

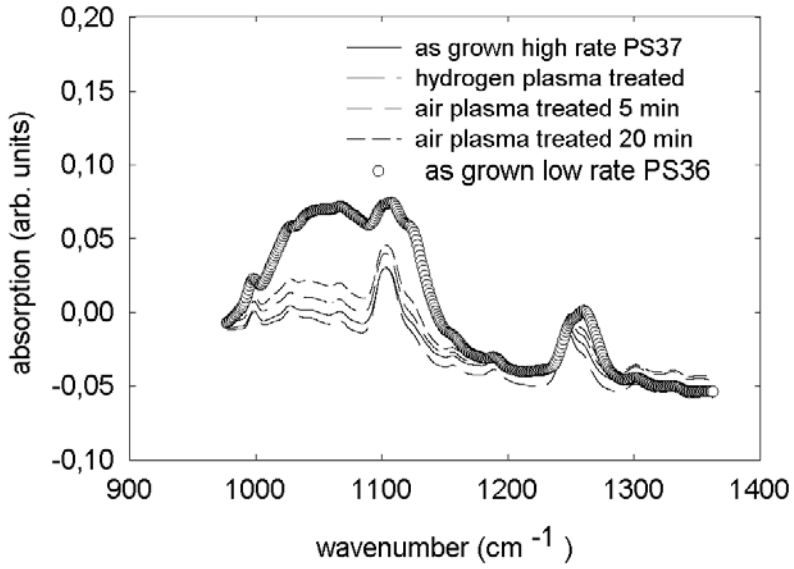

Fig. 3.4 Detail of IR spectra in region of Si–O–Si (1040 cm^{-1}), Si–CH_3 (1247 cm^{-1}) and Si–CH_2–Si (1257 cm^{-1}) of hydrogen and air plasma treated high rate deposited PMPSi films in comparison with a sample prepared at low deposition rate (PSE36)

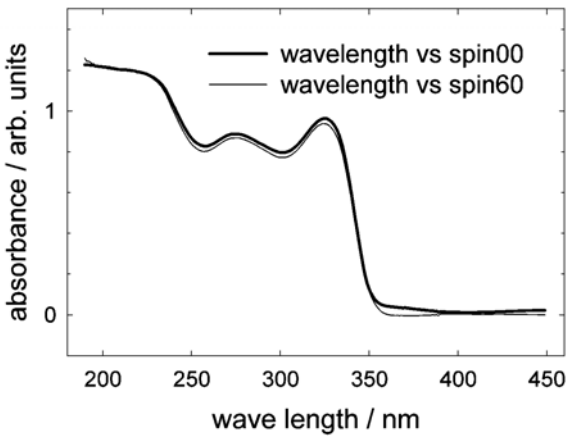

Fig. 3.5 UVVIS spectra of PMPSi layer prepared from the solution by the spin coating method at the incident beam angle 0° and 60°

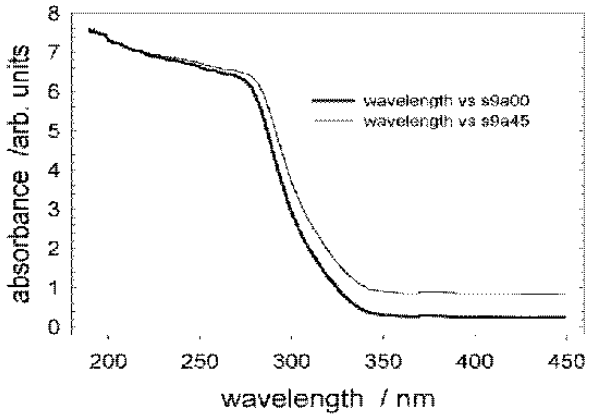

Fig. 3.6 Absorption spectra of evaporated layer of PMPSi (sample 9) prepared at substrate temperature 20°C at incidence beam 0° and 45°

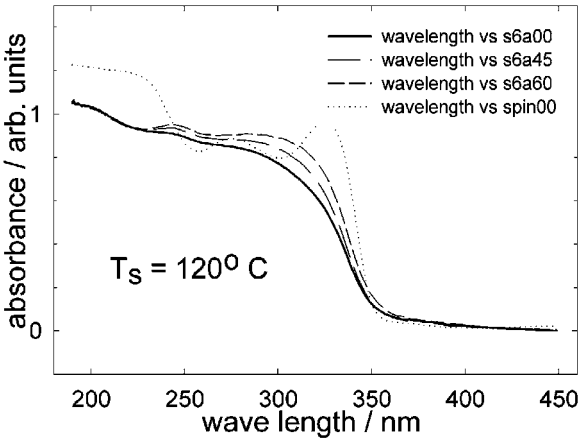

Fig. 3.7 Absorption spectra of a sample prepared on hot substrate (120°C) for angles of light beam incidence – 0°, 45° and 60°

3.2.3 Optical properties

The photon absorption is possible in case when the electrical field of the photon has a non-zero projection into the Si chain direction. For UV radiation parallel with the Si backbone no absorption is expected even in un-polarized case. According to the approach of Takeuchi and Furukawa [48] a perpendicular orientation to the substrate surface of the macromolecule backbone was tested. The samples were measured on a UV VIS spectrometer in the range 450 to 190 nm at incident beam angles of 0°, 45° and 60°. The beam was not polarized, but in case of perpendicular Si backbone orientation increased absorption is expected under oblique beam incidence compared with the perpendicular. No orientation was observed both for the spin coated films and evaporated films at low substrate temperature – see Fig. 3.5 and Fig. 3.6 and a slight orientation effect was observed on the sample prepared on a hot substrate (120°C) – see Fig. 3.7. The measuring error was excluded by comparison with measurements on thin films of PDMSi.

The deposition temperature influences reconstruction of polymer chains on substrates, as apparent from the shift and growth of absorption shoulders.

3.2.4 Luminescence

Luminescence both in steady state and transient regimes was measured by Edinburgh Science FF/FL900, which is able to scan the spectra in the range 200 - 800 nm. The spectral sensitivity of the detector is corrected in the full wavelengths range only for emission measurements, the excitation spectra can be corrected from 230 nm to 800 nm. The influence of Xenon lamps spectral features has been avoided as well [49].

While structurally analogous to saturated hydrocarbons, these polymers show intense near-UV absorption bands attributed to transition between σ-delocalized Si-Si bonding HOMO's and antibonding LUMO's. Moreover, polysilylenes exhibit a high efficient sharp photoluminescence usually in the near UV or UV regions in solid state as well as in a solution.

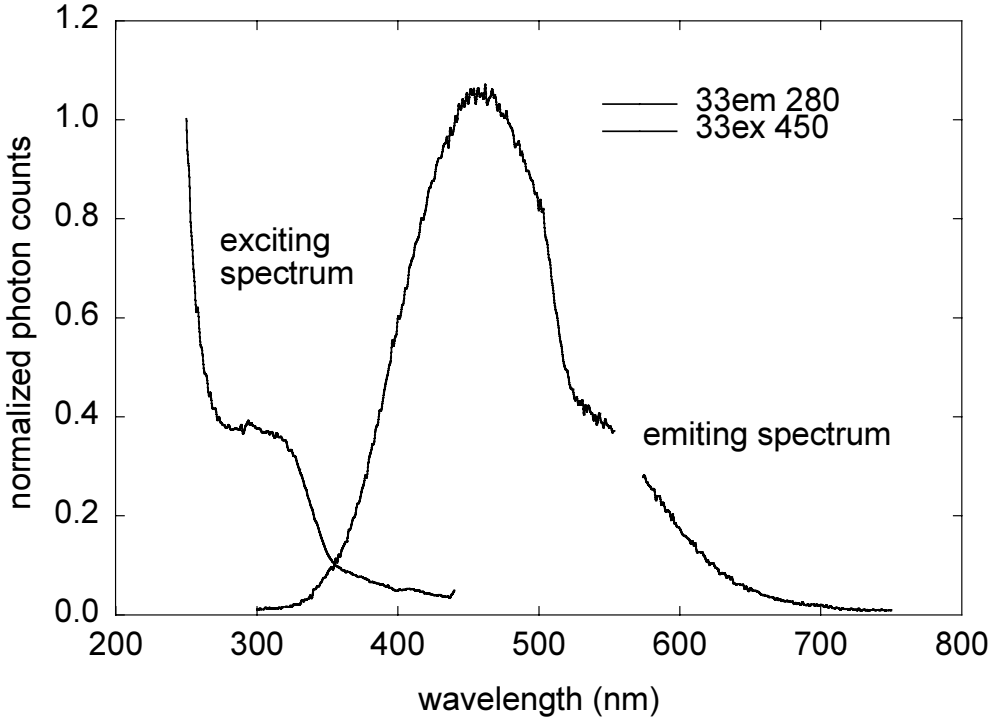

Fig. 3.8 Luminescent spectra of evaporated PMPSi. The emitting spectrum was excited at wavelength 280 nm and excitation spectrum was collected at 450 nm

The PL spectrum of PMPSi has two typical characteristics - the first one is additional broad emission bands in the visible region and the other one is the strong temperature dependence of the visible bands' intensity. When temperature decreases, the intensity of the UV band is changed only slightly, but the visible broadband emission increases continuously. This indicates that the relaxation of the excited states is composed of several competitive processes. It has been revealed that the structural defects of PMPSi act as radiative recombination centers for the luminescence in the visible region. It has been suggested that the PL in the visible region arises from the radiative recombination of excitons localized at branching points in the silicon backbone. The structural defects act as hole traps and the positive space charges then influence the hole transport and the electron injection processes as well. The nature of σ-orbitals is more complicated in PMPSi than in alkyl-substituted polysilylenes because the interaction of π-orbitals of aromatic pendant groups with the delocalized σ-orbitals of the Si chains in PMPSi. The luminescence of evaporated sample – see Fig. 3.8 – exhibit both photoluminescence band at about 360 nm and stronger over coating band with maximum at 460 nm attributed to defect states in the network. It corresponds to short conjugated length of evaporated PMPSi mentioned above.

3.2.5 Electroluminescence

To measure an electroluminescence, an experimental apparatus in UMCH CAS labs in Prague has been built [50]. As a voltage source we used a Keithley 617 electrometer for steady-state measurement or PG 508 pulse generator or HP 408 ac generator for dynamic measurements. A current was measured by Keithley 617 electrometer in steady-state mode or recorded by scope in dynamic regime. An emitted light was detected by a cooled photomultiplier. The output of the photomultiplier was monitored by the picoammeter Keithley 485 or by a scope using a current to voltage converter. To increase the sensitivity of detection of light a combination of a chopper and a lock-in detector was used. The temperature is controlled by a computer using a platinum resistor for detection. The apparatus was constructed as computer controlled. All the devices mentioned above are driven per these interfaces by a controlling program. The program enables measuring by

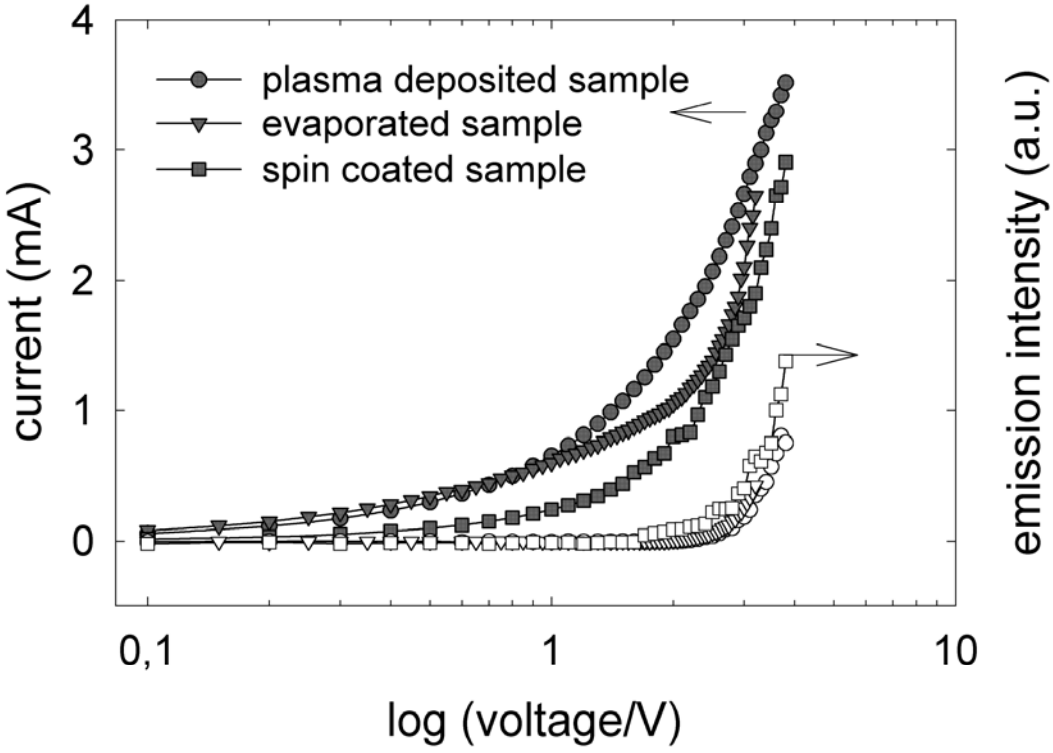

Fig. 3.9 Comparison of the I-V-EL intensity characteristics of PMPSi thin layers prepared by different techniques

using the differential experimental techniques, data acquiring, temperature controlling, saving of experimental data measuring, conditions and setup of devices.

The electroluminescence properties of the evaporated films were investigated. To compare results, EL measurements of the spin coated and plasma deposited thin layers were also carried out. We used an usual configuration of electrodes, an ITO bottom contact as a hole injector, an evaporated Al contact, later Mg-Ag contact, for electron injection for evaporated and spin coated samples, and an Au hole injecting bottom contact and Al electron injecting contact for plasma deposited samples. The sample thickness was usually about 600 nm.

Fig. 3.9 shows typical current-voltage-EL intensity curves for PMPSi single layer LEDs. The LEDs exhibit similar EL intensity characteristics and also the I-V characteristics are comparable. It seems that in all these materials the onset of the EL is primarily determined by the electric field strength in the LED, which depends only on the applied voltage, because the sample thicknesses are the same.

The week electroluminescence of both evaporated and plasma deposited PMPSi disable the spectral measurements. The problems with carrier injection of contacts and dielectric strength of the material were not overcome. The problem was solved later – see chap.3.4.

3.3 ORIENTED THIN FILMS OF PDMSI AND THEIR PROPERTIES

3.3.1 Introduction

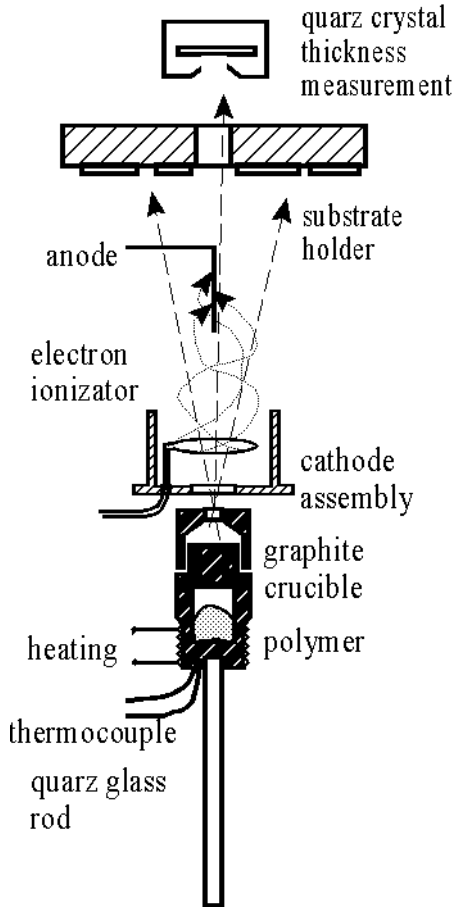

Fig. 3.10 Evaporator assembly with electron cross beam ionization

The chemically prepared poly(dimethylsilylene) (PDMSi) has powder structure. It has bad solubility in any organic solvent; so vacuum deposition as one of the powerful methods to form organic thin films and numbers of studies were published. The first vacuum-deposited poly(dimethylsilylene) was pre-pared by Shimomura et al. (1994) [10]. The low deposition rate at room temperature leads to perpendicular orientation of polymer chains, which can be explored by polarized light. Takeuchi and Furukawa (1995) [51] evaporated poly(dimethylsilane) from a crucible using tungsten wire and irradiation heating of polymer powder. The oriented films with polymer backbone perpendicular to the various surfaces were grown with the deposition rate of 7.0 nm min^{-1}. Doubly oriented PDMSi films were prepared by Hattori at al. (1996) [46] on oriented PTFE substrates coated by the friction. Photo luminescence emission peak shift to higher energy was observed. Resuming the fact that polysilanes being evaporated decompose to oligosilanes consisting of several monomer units, in case of PDMSi is the mean chain length about 10, Ichino et al. in 1996 [11] started to study linear oligosilanes whose chain length was strictly specified to several silicon units. They used permethyldecasilane synthesized in 1996 [52]. It was assigned as MS10.

3.3.2 Preparation technique

PDMSi was prepared in the Institute of Macromolecular Chemistry Czech Academy of Science in Prague by the Wurtz-type reduction method. We used step-by-step four different evaporation deposition methods. Evaporated samples of PDMSi can be divided into four groups.

The first one was from samples PS 40 to PS 47 evaporated from the graphite crucible see Fig. 3.3. The alignment of the PDMSi film was first of all influenced by the deposition rate. Samples prepared at deposition rates above 0.3 nm s^{-1} exhibit according to absorption spectra disordering. The effect of the substrate temperature is less evident, but optimal was the room temperature. Hot substrates create again disordered PDMSi structure. The cross-linking via $–CH_2–$ groups also occurred. It is concluded from the IR 1257 cm^{-1} absorption peak, which increases with the decreasing deposition rate. The mechanical stability of evaporated layer was poor and moreover droplets from melted polymer occurred on substrates.

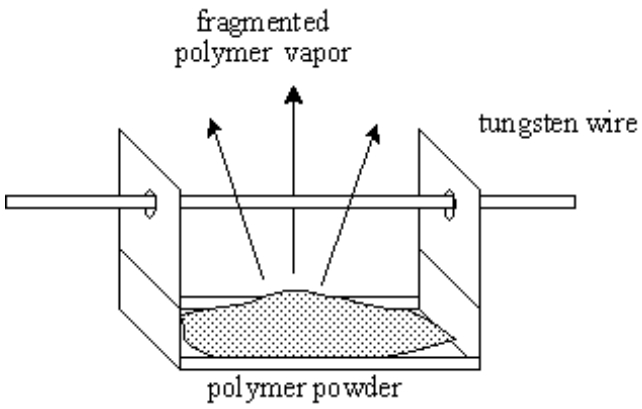

Fig. 3.11 Evaporator with radiative heating

The second one was from PS49 to PS51, where the Knudsen's cell was used, and from

the PS49 sample the electron bombardment of the growing layer was applied - Fig. 3.10. It caused amorphisation of the layer and the exciton photon absorption in 295 nm disappeared. The layer is considered to be crosslinked and the conjugation length of the former oligomer units expired. The exciton absorption extincts if the absorption spectra are measured. The electron bombardment results in films similar to those of plasma deposited.

The third one was from PS52 to PS57, where the crossbeam ionization and excitation of evaporated species were performed. The Knudsen's cell was furthermore used. The optical properties exhibit similar behavior to those of the group one. The layers were softer and tend again

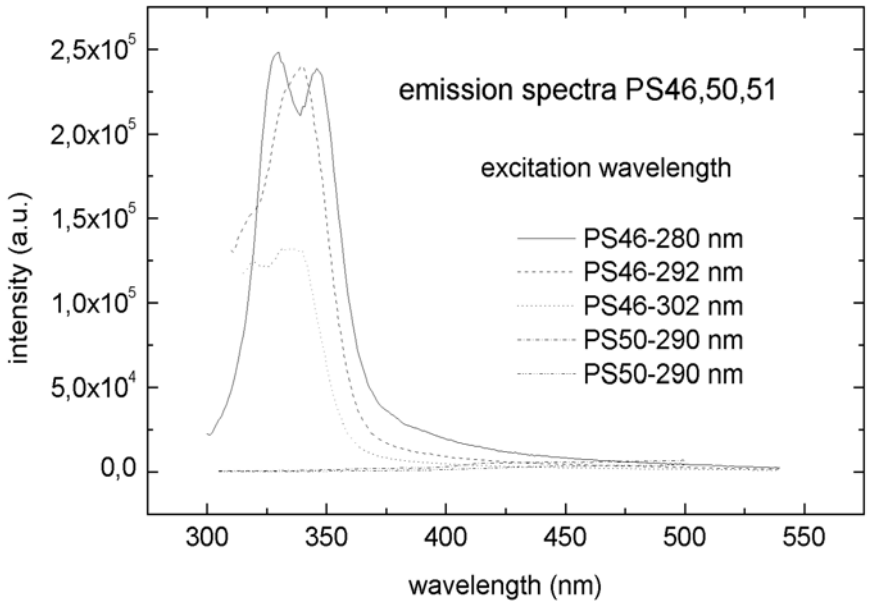

Fig. 3.12 Luminescent emission spectra of evaporated PDMSi (PS46) and evaporated under electron bombardment (PS50)

to recrystalize. It was concluded, that the oligomer conjugation length becomes shorter via multiple contact with hot walls of the Knudsen's cell

The forth group of samples was evaporated by the IR radiation from a hot tungsten filament - Fig. 3.11. The polymer material was heated and evaporated from its surface and no droplets on substrates occurred. It is supposed that the oligomer conjugation length is larger according to better stability of the layer. The mean length of about 10 monomer units is supposed. The oligomer films are partially cross-linked mainly via $–CH_2–$ groups. The dichroism can be observed on perpendicular alignment of the silicon chain to the substrate plane, so the exciton absorption on 295 nm increase with the increasing incident ray angle. The material property according to intensive luminescence is supposed to be convenient for preparation of organic light emitting diodes (OLEDs).

A strong influence of electron beam treatment of the growing layers is apparent. According to absorption spectra the best ordered structure exhibits sample PS46. The peak on the excitation spectra dependence situated near 290 nm corresponds to the exciton creation and it depends strongly on the angle of an incident ray. We consider to have relatively long conjugated length on oligomer chain perpendicular to the substrate surface. Excitation peak 286 nm (photon energy 4.34 eV) corresponds to emitting double peak on 330 and 346 nm (4.1 and 3.91 eV). The splitting of emitting peak is sharply dependent on the excitation length. The emissive intensity is two orders stronger than at samples PS50, 51 prepared under electron beam irradiation. Both samples exhibit damped exciton luminescence but the luminescence on defects becomes more evident. These defects are supposed to be created by electron beam irradiation.

3.4 PREPARATION OF PDMSI ORGANIC LED (OLED)

3.4.1 Indium thin oxide transparent contact

An EL device usually consists of a hole injecting contact, a hole transporting layer, a luminous layer and a metal contact. The barrier height at the hole injecting contact influencing the balance of hole vs electron injection is the parameter affecting the luminous efficiency and device lifetime. For this purpose the work function and surface roughness of the bottom contact have crucial importance for OLED properties. ITO has relatively large work function (between 4 and 5 eV). That is not suitable for many organic materials for the hole injection, so an interlayer of hole injecting polymer and or ITO treatment are used for improvement of its quality.

Kim, J.S. et al (1998) [53] in their excellent study treated commercial ITO films by various methods and they arrived at the main conclusion that oxygen plasma treatment of ITO electrodes before OLED fabrication has the best effect for the work function increase and surface roughness decrease. These results were verified on various OLEDs resulting in efficiency and lifetime improvements. Several kinds of hole transport materials compared Troadec et al. in 2000 [54]: diphenyl-methylphenyl-biphenyl-diamine (TPD), copper phthalocyanine (CuPc), poly(ethylenedioxythiophene) PSS (PEDOT PSS) in tris(hydroxyquinolinate)-d'aluminium (Alq3) based OLED.

On the other hand also the top electron injection cathode plays an important role in the efficiency, stability and lifetime of the device, where the low work function is required. Usually are used Al, Mg (3.7 eV) and Ca (2.9 eV) because of the low work function, but both Mg and Ca need Ag or Al protective layer. In some cases an organic electron transport and injecting layer is also used, the most spread is Alq3 and its derivates. The interlayer avoids also diffusion of metal into the luminous polymer and matches better the interface by lowering the barrier.

We prepared OLED structures consisting of glass (Corning 7059)-ITO-PDMSi-MgAg. Before polymer deposition ITO substrates were tested on surface roughness, we observed the surfaces in the scanning electron microscope (SEM) and the atomic force microscope (AFM) of commercial layers and layers prepared by DC sputtering from ITO target in ISI CAV Brno of RMS roughness not exceeding 1.5 nm. The commercial ITO layer of resistance of 200 Ω exhibits surface grain structure of 100 nm size. After treatment in oxygen plasma the resistance increased up to 2000 Ω and the grain became more evident. Its RMS surface roughness was about 50 nm.

The effect of plasma treatment was tested by contact angle measurements. Water was used as a testing liquid. The contact angle of almost surfaces was between 70° and 90° and as expected after the treatment it fell near to zero. But the differences for various samples occurred after aging. Three kinds of samples were tested. The commercial coarse grained ITO and thin sputtered sample of 300 Ω resistance exhibit after the plasma treatment practically zero contact angle and it remained for 2,000 hours period. The thicker sputtered sample of 20 Ω resistance returned the contact angle above the former value before the treatment. The argon or oxygen ion beam treatment decreases the contact angle to zero, too, but it returns back in few hours. The variation in the behavior of the treated surfaces is not explained and it becomes an object of further study.

The top electrode was double layer of magnesium and silver as a protecting and electron injecting contact. Injection and transport of holes from the positive electrode into the bulk of the polymer film must be matched by injection and transport of electrons from the opposite electrode.

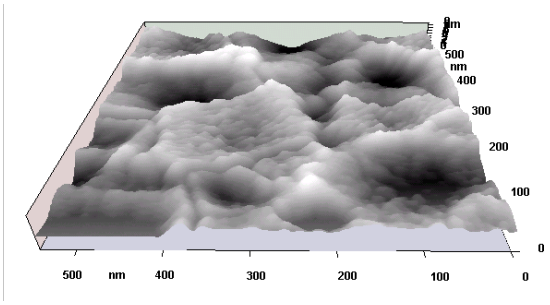

Fig. 3.13 AFM view of ITO layer surface of sample prepared by DC-sputtering method in ISI CAS Brno. The surface RMS roughness is 1.5 nm

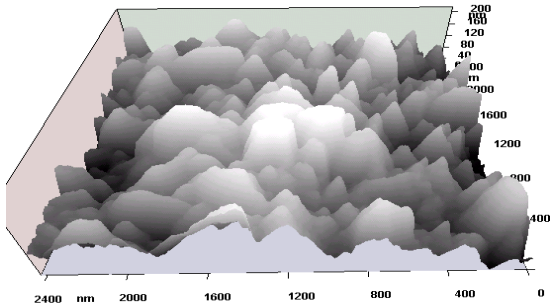

Fig. 3.14 3D view of a commercial ITO of RMS surface roughness 50 nm

We deposited PDMSi films on carefully cleaned ITO surfaces treated in plasma before the deposition. The top electrode we used aluminum, calcium or magnesium. The Mg contact were protected by silver. The magnesium contacts were in some cases better than aluminum, when the barrier limited electron injection occurred. When the current is limited by hole injection or by the space charge, the Al contact was convenient because of its better stability. As the current limiting effect mostly occurred the hole injection from the ITO contact. So an attempt of hole transport and injecting layer copper phthalocyanine (CuPc) was successfully applied.

3.4.2 Electroluminescence (EL)– results and discussion

For electroluminescence measurement some OLED structures were prepared. Corning glass 7059 coated with ITO layer of 200 Ω resistance serves as the substrates. Surface RMS roughness did not exceed 2 nm. Evaporated layers of the thickness from 300 to 400 nm were prepared simultaneously with samples for other measurements. PDMSi layers were covered by strips of Mg-Ag or Al electrodes. The area of the diode was about 1x5 mm. Electroluminescence - voltage dependence comparison of both types contact Low work function material like magnesium starts to inject electrons at much lower voltage then aluminum. The reproducibility of contact effect can be seen by characteristics comparison of four LED structures on the same PDMSi layer. In case of magnesium contact-switching effect can be observed which is considered to be caused by contact barrier forming.

Layers prepared by simple evaporation like PS46 are inconvenient for OLEDs. They have low molecular weight and are soft. The top electrode affects the stress and creep of the polymer layer and shorts under electric field loading. Also, the recrystallization after some days occurs.

The samples prepared under electron beam treatment, which are cross-linked and tough (PS 50,51) exhibit the relatively stable electroluminescence. On the other hand an excess of electron irradiation dose causes degradation of electroluminescence. The shift to higher voltage and noise at both current and luminescence signal reflects the increased concentration of defects. Both the current and electroluminescence yield is limited. The high charge carrier injection cause defect creation in the contact region and subsequent charge capture on these defects. The current is then limited by the space charge on the defect states. The contact barrier height increases the injected carrier energy and the hot carriers contribute to the contact region degradation. The repeated run of V-A measurement is then shifted to higher voltage

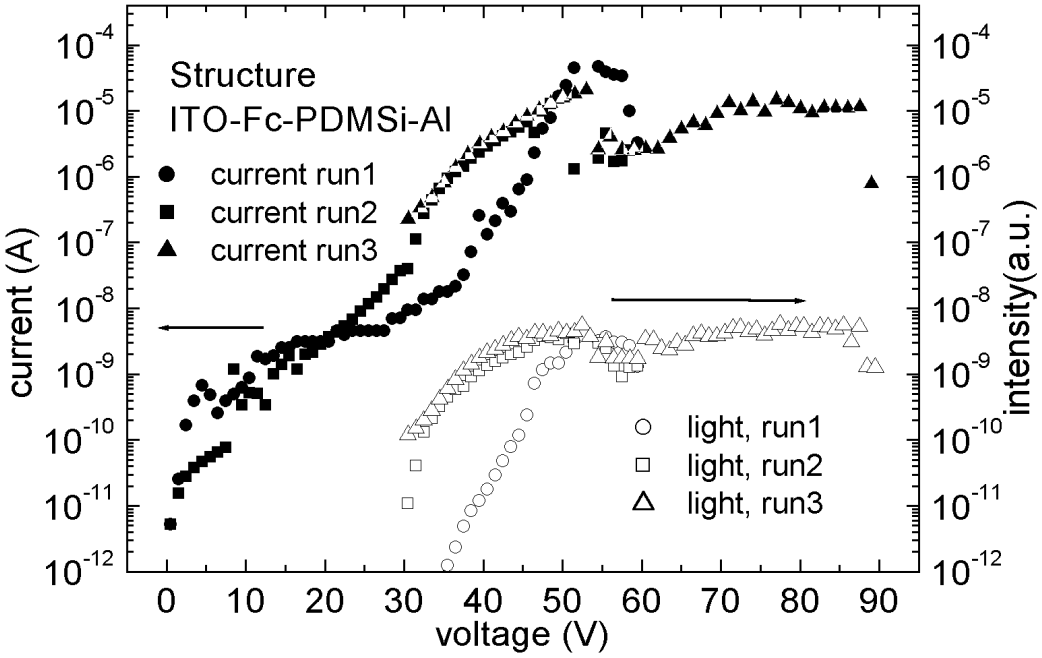

Fig. 3. 1. Electroluminescence from OLED with copper phthalocyanine hole transport and injection layer

The improvement of the electroluminescence yield was achieved by using the copper phthalocyanine hole injection layer between ITO and PDMSi layer – see Fig. 3. 1. It improves hole injection and the radiative recombination region moves towards the electron injection contact. The measurable electroluminescence occurred at three order lower current (10^{-8}A) in comparison with samples without Pc layer and the degradation was suppressed.

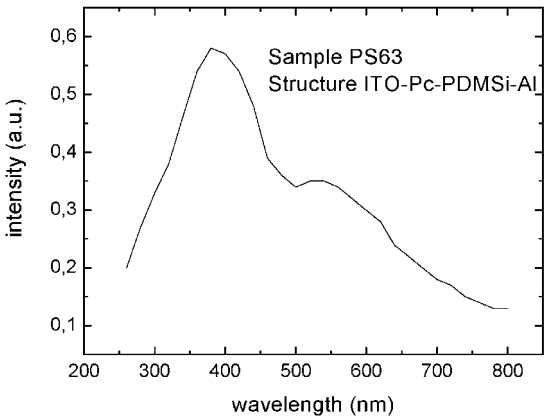

Fig. 3. 2. Electroluminescence spectrum of ITO-PC-PDMSi-Al structure (PS63) OLED

The luminous intensity of PS 63 sample was sufficient for spectral measurement – see Fig. 3. 2. The spectrum consists of two peaks. Both the near UV emission peak with maximum on 380 nm and the green light 520 nm originate from the radiative defect recombination and the exciton recombination exhibits like a shoulder on 300-350 spectral region.

4 SILOXANES BASED COMPOSITE INTERPHASES PREPARED IN PLASMA

A development of high-performance composites is tightly bound with a designing of composite interphases. Silicon based organic interlayers are often used because of their good chemical and thermal stability and environmental safety. Fiber reinforced composites combine high strength of rigid reinforcements with high toughness of flexible matrix. Synergism of the two phases produce mechanical properties of the composite material that cannot be achieved with either of the constituents acting alone, due to the presence of an interphase between the reinforcement and the matrix. Interphases influence and may control the mechanical properties of composites using fibers with a diameter of 5-25 μm and the common fiber volume fraction ranging front 0.5 to 0.7 as it is

evident from experimental and model data. Therefore, the interphase properties are becoming gradually accepted as design and process variables to be tailored for particular end applications [14].

A lot of techniques for surface treatment of fibers are known. They differ depending on the fiber nature (glass, carbon. aramid, polyethylene, etc. [13]. In recent years, plasma techniques found great applications in a development of high-tech composites. Low temperature plasma technology is the new technique used for surface modification of the reinforcements. This technology is able to prepare controlled interphases.

The presented work concerns some plasma techniques topics for glass fiber matching to fiber-reinforced composites. An interlayer Plasma Enhanced Chemical Vapor Deposited (PE CVD) coatings of hexamethyldisiloxane and vinyl-three-etoxysiloxane were prepared and tested. The contribution concerns of the deposition apparatus development and the scratch-tester development for plasma-polymer thin film adhesion examination. The study of discharge composition and time stability was also carried out.

The glass fibers used for composite reinforcement are not convenient for characterization of the plasma polymer coatings. The general coating properties should be tested on planar glass substrates. The apparatus itself should be constructed both for planar substrates and fibers. The deposition conditions in both cases are expected to be similar. For this purpose the rotary

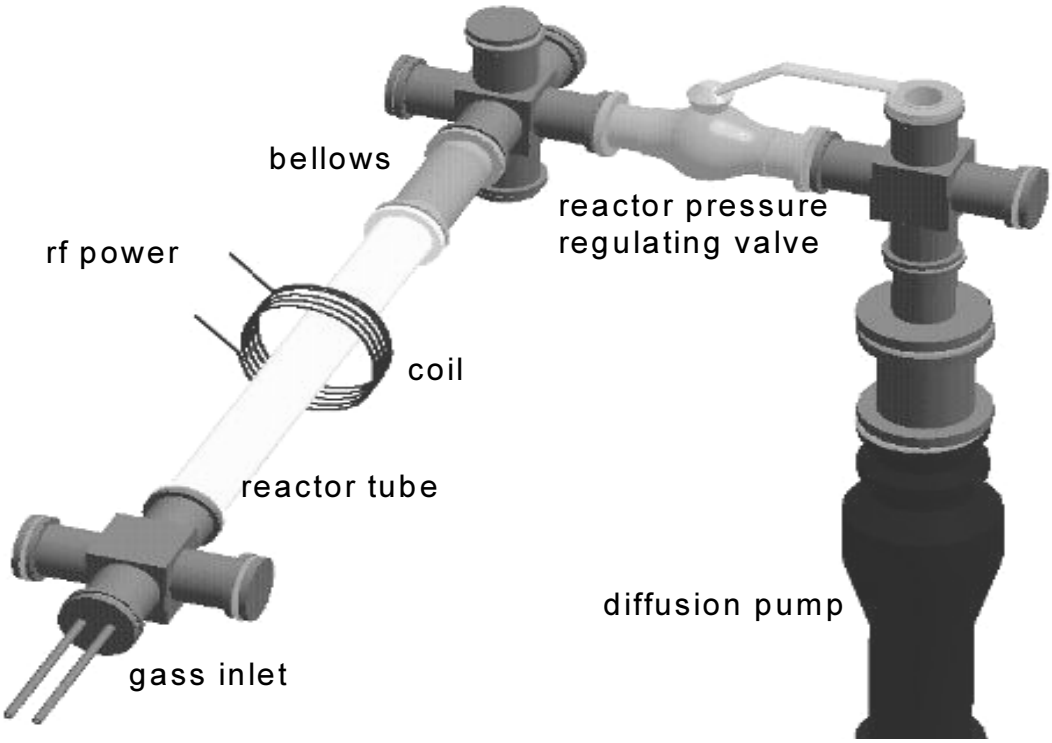

Fig. 4. 1. Schematic view on the vacuum part of the plasma reactor for fiber coatings

symmetric arrangement is chosen. The plasma reactor should be cylindrical and the discharge should be coupled by helical coil round the glass reactor tube. The rf discharge on 13.56 MHz is chosen according to availability of commercial power supplies and other accessories. The vacuum system is also based on commercially available vacuum apparatus AV63 based on classic pumping system (rotary and diffusion pump).

The prepared plasma polymer coatings should be examined on their properties. The basic required property is the good adhesion. For this purpose a scratch – tester was developed and built.

The other optimized quantities are the modulus, inner stress influencing the adhesion and surface wettability influencing the subsequent polymer matrix adhesion in composite. These properties are connected with better available quantities characterizing the deposition conditions and coatings analysis. The mass spectroscopy of plasma composition, the power, pressure and gas flow rates were measured. The prepared samples were examined also on IR absorption spectroscopy, water and other liquids wettability, XPS and some other methods.

My contribution was help with solving the two parts of complex problems concerning the fiber composites research: 1. Design, development and testing of the deposition apparatus for plasma polymer coatings. 2. Design and development of the scratch tester.

4.1 DEPOSITION APPARATUS

The deposition apparatus was developed in two steps. The first variant was simpler and allowed to treat and make coatings on planar substrates and fibers in one charge. The deposition apparatus can be seen in Fig. 4. 1. It was equipped with 100 W/40 MHz rf generator operating in continuous regime. The pressure and the dwelling time were handled both by a ball valve and a gas inlet control flowmeter. The power was regulated by voltage on the power supply ahead of the rf generator. Some experiments on plasma behavior in this system were performed.

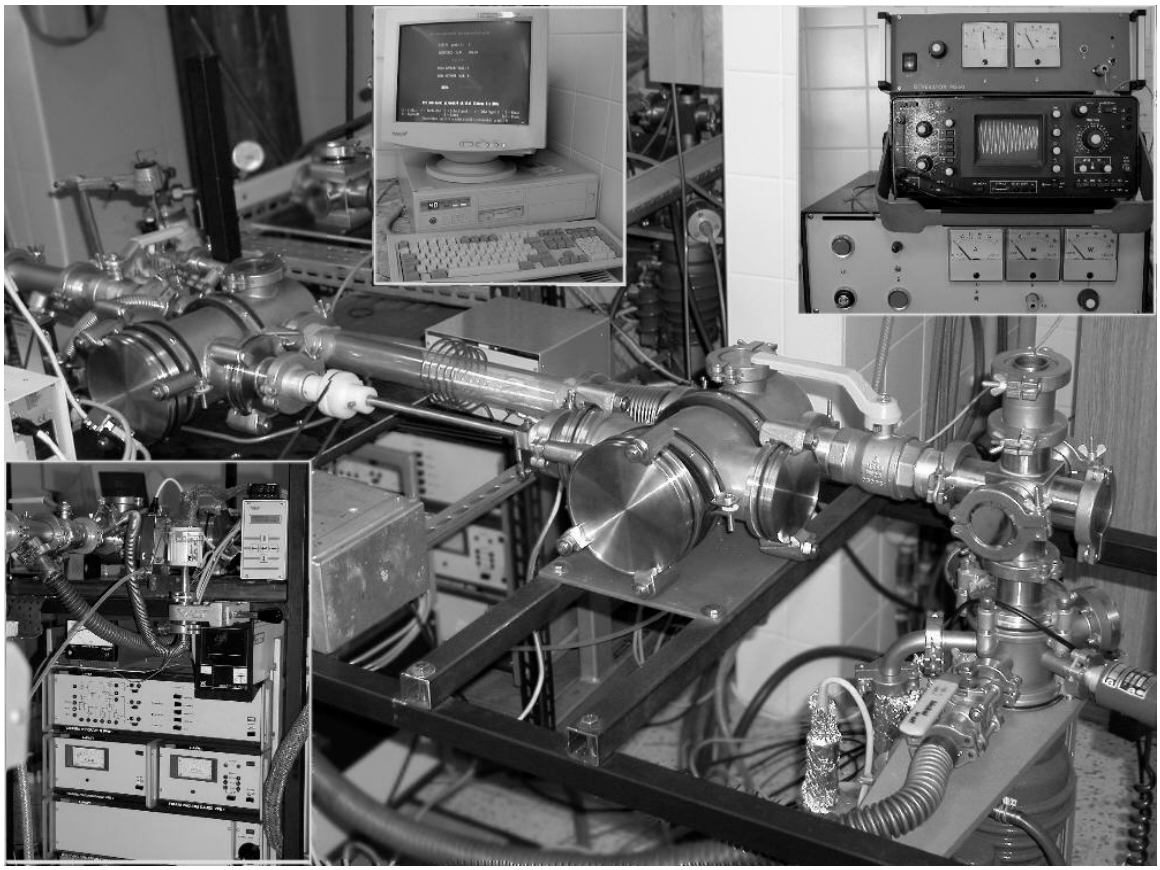

Fig. 4. 2. Apparatus for continuous fiber treatment

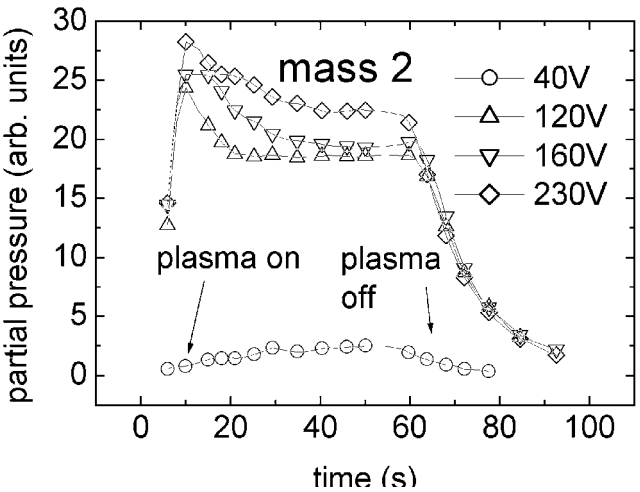

Fig. 4. 4. Time evolution of specie H_2 at plasma switching on and off

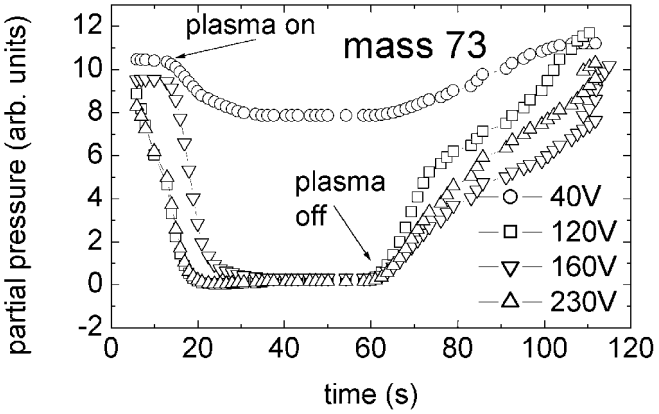

Fig. 4. 3. Time evolution of specie $(CH_3)_3Si$ at plasma switching on and off

The second advanced apparatus was for continuous fiber treatment and was equipped with other accessories for better process control. It is described in [59] and depicted in Fig. 4. 2.

A study of plasma behavior was carried on argon – hexamethyldisiloxane (HMDSO) mixture. The polymerization of hexamethyl-disiloxane (HMDSO) in plasma brings some troubles by deposition on the inner surfaces of the reactor. The reactions in discharge are different from those in the afterglow plasma. At first the main reactions split the bonds by collisions with electrons with wide distributed energies. Then afterglow plasma reactions are initialized by the metastable particles (so called Penning transfer) with specific energy and the bond breaking is better defined. So the streaming is directed to comparison of layers creation in the afterglow region with those prepared in the center of discharge. The results are presented in [60].

The discharge can burn in two modes. The helical coupled plasma behaves in that case like capacitively coupled discharge where the rf coil is one electrode and the grounded metal parts of the apparatus serve as the opposite electrode. At higher rf power it switched into the mode where the induced coupled plasma is supposed. The most of depositions were performed in the second mode with dense plasma localized inside the rf coil.

The high power mode was investigated by detail with use of mass spectroscopy. The influence of monomer input location at various pressures and gas flow rates was tested. The conditions for afterglow decomposition of HMDSO should prevent monomer from getting into the discharge zone. The pressure and the main flow velocity of argon do not allow monomer to diffuse into the discharge. Some calculation were done to solve this problem theoretically and some attempts were performed.

Then the attempt answering time evolution of plasma composition was carried out. Mass spectrometer was switched in regime of partial pressure observation and time dependencies of selected mass (H_2^+, CH_3^+ and mass 73 – prevailed specie $(CH_3)_3Si$) were taken as representatives for typical behavior. The time response on plasma switch on and off was taken on Fig. 4. 4, Fig. 4. 3. Fig. 4. 4 shows time evolution of hydrogen in monomer passing through the discharge. This effect explains one aspect of layer growth. The dangling bonds of the deposited layer are passived by hydrogen. The hydrogen deficit product layers with dangling bonds and internal stress and its excess terminates polymer radicals existence. Similar behavior was observed at methyl radicals.

The evolution of fragment with mass number 73 has inverted behavior in comparison to hydrogen - Fig. 4. 3. Low power produces slow concentration decrease after plasma ignition. Slow concentration increase after plasma quenching is caused by sorption and pumping effect of freshly deposited and active layer.

4.2 SCRATCH TESTER

One of indirect method for adhesion determination is the scratch test based on determination of the critical load L_c for thin film peeling. The Rockwell ball or a diamond tip of defined radius moves along the surface while the load is increased. The created notches are observed by a microscope. The critical load is than appointed by help of comparison of the tangential force record, which is measured as well, and the microscope image.

The detail description of the scratch tester was published in [61].

The support of the following grant is acknowledged:

1. Grant VA Brno G93/12, „Amorfní hydrogenovaný křemík pro aplikaci v ekologii“
2. GAČR 102/96/0105 „Vývoj tenkovrstvého tranzistoru řízeného polem na bázi organických látek“
3. GA ČR 104/00/0708, 2000-2002, „Plazmatické povrchové úpravy skleněných vláken pro polymerní kompozity“
4. Desorpce vodíku z vrstev a-Si:H, Zpráva č.17 Grant VA G92/21, Brno (1992), 17,
5. Grant VA Brno G93/12, „Amorfní hydrogenovaný křemík pro aplikaci v ekologii“
6. GAČR 102/96/0105 „Vývoj tenkovrstvého tranzistoru řízeného polem na bázi organických látek“
7. GAČR 102/96/0105 „Vývoj tenkovrstvého tranzistoru řízeného polem na bázi organických látek“
8. Academy of Sciences Grant Agency contract GAAV A4050603 „Polymerní látky pro fotoelektricky aktivní detektory“
9. Academy of Sciences Grant Agency contract A 1050901: „Proudový modulátor založený na molekulárním vodiči s bočními fotochromními skupinami“
10. COST 518 – grant EU základního výzkumu „Vacuum and plasma deposition of functional molecular materials – electronic structure, transport and luminescence“
11. Czech Grant agency contract 202/00/518: „Metastabilita v organokřemíkových strukturách s proměnnou dimenzionalitou“

REFERENCES

[1] Stearling H. F. and Swann R.C.G.: *Silid State Electronics,* **8**(1965), 653

[2] Spear, W. E.,. LeComber, P. G *Phil. Mag.* **33**(1976) 935

[3] Mishima Y., Hirose M. and Osaka Y.: *Jpn. J. Appl. Phy.,* 22(1983), 2

[4] Matsuo S. and Kiuchi M.: *Jpn. J. Appl. Phys.* 22(1983), L210

[5] Kaufmann, R. H, Robinson, R. S.: *AIAA Journal* **20** (1982), 745.

[6] Pope M., Kallman H. P., Magnante P.: *J. Chem. Phys.*, vol. 38(1963), p. 2042-2048

[7] Tang C. W. and Van Slyke S. A.: *Appl. Phys. Lett.*, vol. 51(1987), no. 12, p. 913-915

[8] Adachi C., Tokito S., Tsutsui T., Saito S. *Jpn. J. Appl. Phys.*, vol. 27(1988), no. 4, p. 713-715

[9] Sheats J. R., Antoniadis H, Hueschen M, Leonard W, Miller J, Moon R, Roitman D, Stocking A.: *Science*, vol. 273(1996), no. 5277, p.884-888

[10] Shimomura, M., Ueno, K., Okumoto,H., Shen, J. and Ito, K. *Macromolecules*, **27**, (1994)7006

[11] Ichino I., Minami N., Yatabe T., Shimomura M and Kaito A.: *Synthetic Metals* **101** (1999), 637

[12] L. H. Sharpe, “Interfaces, interphases and adhesion: a perspective”. *Proc. NATOASI The Interfacial Interactions in Polymeric Composites,* (Ed. G. Akovali). Arrtalya/ Kemer, Kluwcr Academic Publ., 1993. pp. 1-20

[13] J-K. Kim and Y-W. Mai, Engineered Interfaces in Fibre Reinforced composites, Amsterdam. Elsevier 1998

[14] J-K. Kim and Y-W. Mai, “Interfaces in composites”, *Structure and Properties of Fibre Composites* (Ed. T.W. Chou), Series Vol.13, VCH Publishers, 1993, pp.-239-289

[15] Staebler, D.L, Wronski, C.R., *J. Appl. Phys.* **51**(1980) 3262

[16] Jackson, W. B. and Zhang, S.B., in *Transport Correlation and Structure Defects.* (Fritzsche, H., Editor.) P. 63, 128. World Scientific Publishing Company, New York, 1990

[17] Asmussen J.: *J.Vac. Sci. Technol.* **A7** (1989), 883

[18] Musil, J., Žáček, F.: Experimental Study of the Absorption of Intense Electromagnetic Waves in a Magnetoactive Plasma. *Rozpravy ČSAV*, Academia Praha, 1975

[19] Šícha M.: Effect of Collisions on the Charged Particles Collection by a Langmuir Probe., *Sborník VI. Symposia elementárnych procesoch a chemických reakciách v nízkoteplotnej plazme,* Bratislava, JSMF 1988

[20] Goodyear C. C., von Engel A., *Proc. Phys. Soc.* **79** (1962), 732

[21] Waibel H.: PhD Thesis, Universitat Kaiserslautern D386, 1988

[22] Bennet J. E. and Blackmore D. R., *Proc. R. Soc. London,* Ser. **A 305**

[23] Kiel R.E., *AIAA Journal* **6**, No. 4, 1967

[24] Iselborn, S., Rübel, H., Geiger, J., Schröder B.: *Phil. Mag.* **B48**(1983) 561

[25] Anderson, J. C., Biswas, S.: *J. Non-Cryst Solids*, **77/78**(1985) 817

[26] Shindo, M., Sato, S., Myokoan, I., Mano, S., Shibata, T.: *J. Non-Cryst. Solids* **59/60**(1983) 747

[27] Grasso, V., Mezzasalma, A.M., Neri, F. : *Solid State Commun.* **41**(1982) 675

[28] Yamada, H. Inokawa and T. Takagi *J. Appl. Phys.* **56** (1984), p. 2746

[29] Salyk O., PhD Thesis, Technical Academy, Brno 1987

[30] Poruba A.: Doktorská disertační práce. FCH VUT, Brno 1998

[31] Zhank M. and Nakayama Y.: *Solid State Phenom.* **44-46** (1995), 135

[32] Beyer W.: *J. Non-Cryst. Sol.*, **198-200** (1996)

[33] Cai-Zou-Tao, He-Ke-Lun, Li Zhi-an, Cheng Ru-Guang: *Solar Energy Materials* **12** (1985), 43

[34] Barret P. Reakce pevná látka-plyn. Academia, Praha 1978

[35] Websites fy Netzsch http://www.ngb.netzsch.com/sta409pc.htm

[36] Dixmier J., Derouet P., Essamet M., Laridiani M.: *Phil. Mag.* **B 52** (1985), 943

[37] Zanzucchi P. J.: In: "*Semiconductors and Semimetals*", vol. **21B**, ed. by Pankove J. I., Academic Press, Inc. (1984), 113

[38] Stuchlík, J., *PhD. Thesis*. Institute of Physics CAS, Prague, 1994

[39] Poruba, O. Salyk, P. Horváth and F. Schauer: A Proceeding of 9th International School on Condensed Matter Physics: A Future Direction in Thin Film Science and Technology, September 9th-13th, 1996, Varna, Bulgaria

[40] Luterová, K., Poruba, A., Dian, J., Salyk, O., Horváth, P., Knápek, P., Valenta, J., Kočka, J., Pelant, I. Journal of Porous Materials, 2000, vol. 7, p. 135 –138

[41] Miller R. D. and Michl J., *Chem. Rev.* **89,** (1989), 1359

[42] West R. *J. Organomet. Chem.* **300**(1986), 327

[43] Zhang X. H. and West R.: *J. Polym. Sci.: Polym. Chem Ed.* **22** (1984), 159

[44] M. Shimomura, K. Ueno, H. Okumoto, J. Shen and K. Ito, *Macromolecules*, **27**, 7006.1994

[45] T. Yatabe, M. Shimomura and A. Kaito, *Chemistry Letters* **1996**, 551

[46] R. Hattori, T. Sugano, J. Shirafuji, and T. Fujiki, *J. Appl. Phys*. Vol. **35**, pp. L 1509,1996

[47] H. K. Kim and K. Matyjaszewski, *J. of Polymer Science: Pt. A: Polymer Chemistry*, Vol. **31**, 299,1993

[48] K. Takeuchi and S. Furukawa, *Jpn .J. Appl. Phys*. Vol. **34** Pt. 2. L 195, 1995

[49] Horváth P.: *PhD Thesis ,* Brno 2001

[50] Weiter M.: *PhD Thesis ,* Brno 2001

[51] Takeuchi Ken-ichiro and Furukawa Shoji, *Jpn. J. Appl. Phys.* **34** (1995), Pt.2. No. 2A, L196.

[52] Yatabe T., Shimomura M. and Kaito A.: *Chem. Lett.*(1996), 551

[53] Kim, J. S., Grandröm, M., Friend, R. H., Johansson, N., Salaneck, W. R., Daik, R., Feast, W. J., and Cacialli, F.: In: *J. Appl. Phys*. **84**(1998), 6859-6870

[54] Troadec D., Veriot G., Antony R. and Moliton A., *Synthetic Metals* Volume **124**, Issue 1, 3 October 2001, Pages 49-51

[55] Schauer F., Nešpůrek S., Horváth P., Zemek J., Fidler V.: *Synthetic Metals* **109**, 321 - 325(2000)

[56] Nespurek, S., *Macromol.Symp.* **104**(1996), 285.

[57] E. Brynda, I. Koropecký, I. Kmínek, S. Nešpůrek and W. Schnabel. *Polym. Adv. Technol.* **5** (1993), p. 257

[58] Cech V. : *Proc. 8th Int. Conf. On Fibre Reinforced Composites FRC 2000* (ed. By A. G. Gibson), Woodhead Publishing Ltd. Cambridge (2000), pp 246-251

[59] Prikryl R., Salyk, Vanek J., Studynka J. and Cech V. *Czech. J. Phys,* **52** (2002), D816

[60] Balkova, R, Prikryl, R., Cech, V. and Salyk, O. In *Proc.15th International Symposium on Plasma Chemistry, Volume V, Poster Contributions*, Gremi, CNRS/ Edited by A. BOUCHOULE, J. M. POUVESLE, A. L. THOMANN, J. M. BAUCHIRE AND E. ROBERT, University of Orléans, 9-13 July 2001, France, pp. 1747-1753

[61] Prikryl R., Salyk O., Kripal L., Cech V.: *Czech. J. Phys,* **52** (2002), D824

ABSTRACT

Presented work is devoted to four continuing themes of thin films preparation and vacuum and plasma technology acquired in plasma laboratory of the faculty workplace. All these topics concern silicon based compounds and are joined by common methods of preparation and examination. The emphasis is directed on preparation techniques, where the vacuum and plasma technologies prevail. Several original equipments for thin films deposition and testing were developed for this reason and are described: microwave magnetoactive plasma source, microwave magnetoactive ion source, apparatus for hydrogen plasma assisted electron beam evaporation with specially designed electron gun, apparatus for temperature control and data acquisition of the thermal desorption spectroscopy, evaporator assembly with electron cross beam ionization, the plasma reactor for fiber coatings, apparatus for continuous fiber treatment, scratch tester and some other small devices. The thesis contains also the main results acquired by designed equipments and devices like measured properties of amorphous hydrogenated silicon, polymethylphenylsilane, polydimethylsilane and polymethylsiloxane thin films.

ABSTRAKT

Práce je věnována čtyřem navazujícím tématům přípravy tenkých vrstev a plazmatických a vakuových technologií vyvinutých v laboratoři plazmatu na pracovišti fakulty. Všechna tato témata se týkají sloučenin na bázi křemíku a jsou provázána společnými metodami přípravy a měření. Důraz je kladen na postupy přípravy, kde převládají vakuové a plazmatické technologie. Byla vyvinuta řada přístrojů, zařízení a přípravků pro depozice tenkých vrstev a jejich testování jako například: mikrovlnný magnetoaktivní zdroj plazmatu, mikrovlnný magnetoaktivní zdroj iontového svazku, zařízení pro napařování elektronovým dělem v prostředí vodíkového plazmatu, vlastní elektronové dělo, zařízení pro tepelnou desorpční analýzu - řízení teploty a sběr dat, odpařovadlo s ionizací příčným elektronovým svazkem, plazmatický reaktor pro povlakování vláken, zařízení pro kontinuální povrchovou plazmatickou úpravu vláken a další menší zařízení a přípravky. Téze obsahuje rovněž nejvýznamnější výsledky získané na vyvinutých zařízeních jako změřené vlatnosti tenkých vrstev amorfního hydrogenovaného křemíku, polymetyl-fenylsilanu, polydimetylsilanu a plazmatického polymetylsiloxanu.